Historical and idealized climate model experiments: an intercomparison of Earth system models of intermediate complexity

Clim. Past, 9, 1111–1140, 2013
www.clim-past.net/9/1111/2013/
doi:10.5194/cp-9-1111-2013

Climate of the Past
Open Access

Historical and idealized climate model experiments: an intercomparison of Earth system models of intermediate complexity

M. Eby[1], A. J. Weaver[1], K. Alexander[1], K. Zickfeld[2], A. Abe-Ouchi[3,4], A. A. Cimatoribus[5], E. Crespin[6], S. S. Drijfhout[5], N. R. Edwards[7], A. V. Eliseev[8], G. Feulner[9], T. Fichefet[6], C. E. Forest[10], H. Goosse[6], P. B. Holden[7], F. Joos[11,12], M. Kawamiya[4], D. Kicklighter[13], H. Kienert[9], K. Matsumoto[14], I. I. Mokhov[8], E. Monier[15], S. M. Olsen[16], J. O. P. Pedersen[17], M. Perrette[9], G. Philippon-Berthier[6], A. Ridgwell[18], A. Schlosser[15], T. Schneider von Deimling[9], G. Shaffer[19,20], R. S. Smith[21], R. Spahni[11,12], A. P. Sokolov[15], M. Steinacher[11,12], K. Tachiiri[4], K. Tokos[14], M. Yoshimori[3], N. Zeng[22], and F. Zhao[22]

[1]School of Earth and Ocean Sciences, University of Victoria, Victoria, British Columbia, Canada
[2]Simon Fraser University, Vancouver, British Columbia, Canada
[3]Atmosphere and Ocean Research Institute, The University of Tokyo, Kashiwa, Japan
[4]Research Institute for Global Change, Japan Agency for Marine-Earth Science and Technology, Yokohama, Japan
[5]Royal Netherlands Meteorological Institute, De Bilt, the Netherlands
[6]Georges Lemaître Centre for Earth and Climate Research, Université Catholique de Louvain, Louvain-La-Neuve, Belgium
[7]The Open University, Milton Keynes, UK
[8]A. M. Obukhov Institute of Atmospheric Physics, RAS, Moscow, Russia
[9]Potsdam Institute for Climate Impact Research, Potsdam, Germany
[10]Pennsylvania State University, Pennsylvania, USA
[11]Climate and Environmental Physics, Physics Institute, University of Bern, Bern, Switzerland
[12]Oeschger Centre for Climate Change Research, University of Bern, Bern, Switzerland
[13]The Ecosystems Center, MBL, Woods Hole, Massachusetts, USA
[14]University of Minnesota, Minneapolis, Minnesota, USA
[15]Massachusetts Institute of Technology, Cambridge, Massachusetts, USA
[16]Danish Meteorological Institute, Copenhagen, Denmark
[17]National Space Institute, Technical University of Denmark, Kgs. Lyngby, Denmark
[18]School of Geographical Sciences, University of Bristol, Bristol, UK
[19]Department of Geophysics, University of Concepcion, Concepcion, Chile
[20]Niels Bohr Institute, University of Copenhagen, Copenhagen, Denmark
[21]National Centre for Atmospheric Science – Climate, University of Reading, Reading, UK
[22]University of Maryland, College Park, Maryland, USA

Correspondence to: M. Eby (eby@uvic.ca)

Received: 27 July 2012 – Published in Clim. Past Discuss.: 28 August 2012
Revised: 8 March 2013 – Accepted: 13 March 2013 – Published: 16 May 2013

Abstract. Both historical and idealized climate model experiments are performed with a variety of Earth system models of intermediate complexity (EMICs) as part of a community contribution to the Intergovernmental Panel on Climate Change Fifth Assessment Report. Historical simulations start at 850 CE and continue through to 2005. The standard simulations include changes in forcing from solar luminosity, Earth's orbital configuration, CO_2, additional greenhouse gases, land use, and sulphate and volcanic aerosols. In spite of very different modelled pre-industrial global surface air temperatures, overall 20th century trends in surface air temperature and carbon uptake are reasonably well simulated when compared to observed trends. Land carbon fluxes show much more variation between models than ocean carbon

Published by Copernicus Publications on behalf of the European Geosciences Union.

fluxes, and recent land fluxes appear to be slightly underestimated. It is possible that recent modelled climate trends or climate–carbon feedbacks are overestimated resulting in too much land carbon loss or that carbon uptake due to CO_2 and/or nitrogen fertilization is underestimated. Several one thousand year long, idealized, $2\times$ and $4\times CO_2$ experiments are used to quantify standard model characteristics, including transient and equilibrium climate sensitivities, and climate–carbon feedbacks. The values from EMICs generally fall within the range given by general circulation models. Seven additional historical simulations, each including a single specified forcing, are used to assess the contributions of different climate forcings to the overall climate and carbon cycle response. The response of surface air temperature is the linear sum of the individual forcings, while the carbon cycle response shows a non-linear interaction between land-use change and CO_2 forcings for some models. Finally, the preindustrial portions of the last millennium simulations are used to assess historical model carbon-climate feedbacks. Given the specified forcing, there is a tendency for the EMICs to underestimate the drop in surface air temperature and CO_2 between the Medieval Climate Anomaly and the Little Ice Age estimated from palaeoclimate reconstructions. This in turn could be a result of unforced variability within the climate system, uncertainty in the reconstructions of temperature and CO_2, errors in the reconstructions of forcing used to drive the models, or the incomplete representation of certain processes within the models. Given the forcing datasets used in this study, the models calculate significant land-use emissions over the pre-industrial period. This implies that land-use emissions might need to be taken into account, when making estimates of climate–carbon feedbacks from palaeoclimate reconstructions.

1 Introduction

Climate models are powerful tools that help us to understand how climate has changed in the past and how it may change in the future. Climate models vary in complexity from highly parameterized box models to sophisticated Earth system models with coupled atmosphere–ocean general circulation model (AOGCM) subcomponents, such as those involved in the Coupled Model Intercomparison Project Phase 5 (CMIP5; Taylor et al., 2012). Different models are designed to address different scientific questions. Simple models are often useful in developing and understanding individual processes and feedbacks, or teasing apart the basic physics of complex systems. However, they usually lack the complex interactions that are an integral part of the climate system. Current "state-of-the-art" Earth system models are both sophisticated and complex, but the number and length of simulations that can be performed is limited by the availability of computing resources. Another class of models, known as Earth system models of intermediate complexity (EMICs), helps fill the gap between the simplest and the most complex climate models (Claussen et al., 2002).

Usually EMICs are complex enough to capture essential climate processes and feedbacks while compromising on the complexity of one or more climate model component. Often EMICs are used at lower resolution, and model components may have reduced dimensionality. While generally simpler, EMICs sometimes include more subcomponent models than Earth system AOGCMs. New subcomponents (for example, continental ice sheets, representations of peatlands, wetlands or permafrost) are often developed within the EMIC framework before they are embedded into coupled AOGCMs, because development and testing is less computationally expensive. In addition, there are some processes operating within the Earth system (e.g. carbonate dissolution from sediments or chemical weathering) with very long inherent timescales that can only be integrated by EMICs.

With relatively abundant proxy data, the last millennium is an important test bed for validating the longer term climate–carbon response of models. Understanding the role of climate forcing over this period will help to reconcile any inconsistences between the models and the various palaeo-forcing and data reconstructions and improve our confidence in future simulations. There are a very limited number of studies that have modelled the climate–carbon cycle response over this period (Gerber et al., 2003; Goosse et al., 2010; Jungclaus et al., 2010), and while a few AOGCMs have carried out climate simulations over the last millennium (for example, González-Rouco et al., 2003; Jungclaus et al., 2010; Swingedouw et al., 2010; and Fernández-Donado et al., 2012), these studies were limited in the number of experiments that could be performed. See Fernández-Donado et al. (2012) for a comprehensive review of the current state of climate simulation and reconstruction over the last millennium.

Given their relatively rapid integration times, EMICs are capable of simulating climate change over many thousands of years. They are able to perform the many simulations needed to investigate the sensitivity of climate to various external forcings. EMICs often have relatively low levels of internal variability, which makes them particularly useful in experiments investigating the forced response of the climate system. Many EMICs also include long timescale carbon processes such as changes in carbonate sedimentation, wetlands or permafrost, processes which are usually missing in models designed for shorter simulations. These characteristics make EMICs particularly well suited to investigate the forced climate–carbon response over the last millennium.

Over the years a number of model intercomparison projects have been designed using EMICs (e.g. Pethoukhov et al., 2005; Rahmstorf et al., 2005; Brovkin et al., 2006; Plattner et al., 2008). More typically, however, EMICs have been included in model intercomparisons with coupled AOGCMs (e.g. Gregory et al., 2005; Stouffer et al., 2006; Friedlingstein et al., 2006). Results from EMIC simulations

were used extensively in the Intergovernmental Panel on Climate Change (IPCC) Fourth Assessment Report (AR4; IPCC, 2007). As part of the EMIC community's contribution to the Fifth Assessment Report, 15 EMICs have contributed results from a series of experiments designed to examine climate change over the last millennium and to extend the representative concentration pathways projections that are being simulated by the CMIP5 models.

This paper summarizes the results of historical and idealized experiments. The climate and carbon cycle response of models over the historical period are compared to observational estimates. Idealized experiments are used to generate climate and carbon cycle metrics for comparison with previous studies or results from other models. The historical climate response is presented in Sect. 3.1 and idealized climate metrics in Sect. 3.2. The historical carbon response is discussed in Sect. 3.3 and idealized carbon metrics in Sect. 3.4. Historical experiments that were used to explore the contributions of various specified forcings over the last millennium are described in Sect. 3.5 and the linearity of the response in Sect. 3.6. Contributions of natural and anthropogenic forcings to the climate response are compared in Sect. 3.7. The preindustrial portion of the last millennium is also used to assess changes in temperature in Sect. 3.8, changes in CO_2 in Sect. 3.9, and the climate–carbon cycle sensitivity in Sect. 3.10. Details of experiments that explore future climate change commitment and irreversibility can be found in Zickfeld et al. (2013).

2 Experimental design

2.1 Models

Fifteen EMICs participated in this intercomparison project. The participating model names with version numbers, followed by a two-letter abbreviation (in parentheses), and contributing institution, are as follows: Bern3D (B3) from the University of Bern; CLIMBER-2.4 (C2) from the Potsdam Institute for Climate Impact Research; CLIMBER-3α (C3) from the Potsdam Institute for Climate Impact Research; DCESS v1 (DC) from the Danish Center for Earth System Science; FAMOUS vXFXWB (FA) from the University of Reading; GENIE release 2-2-7 (GE) from The Open University; IAP RAS CM (IA) from the Russian Academy of Sciences; IGSM v2.2 (I2) from the Massachusetts Institute of Technology; LOVECLIM v1.2 (LO) from the Université Catholique de Louvain; MESMO v1.0 (ME) from the University of Minnesota; MIROC-lite (MI) from the University of Tokyo; MIROC-lite-LCM (ML) from the Japan Agency for Marine-Earth Science and Technology; SPEEDO (SP) from the Royal Netherlands Meteorological Institute; UMD v2.0 (UM) from the University of Maryland; and UVic v2.9 (UV) from the University of Victoria. Model characteristics are compared in Table 1, and more complete descriptions are provided in Appendix A. Unlike the EMICs cited in the AR4, several models now calculate land-use change carbon fluxes internally (B3, DC, GE, I2, ML, UV) and/or include ocean sediment and terrestrial weathering (B3, DC, GE, UV). Eight EMICs (B3, DC, GE, I2, ME, ML, UM and UV) include interactive land and ocean carbon cycle components that allow them to diagnose emissions that are compatible with specified CO_2 concentrations.

2.2 Methods

To be consistent with other intercomparison projects, forcing for the initial condition and the historical period were obtained from the Paleoclimate Modelling Intercomparison Project Phase 3 (PMIP3) and CMIP5-recommended datasets. Specified forcings included orbital configuration (from Berger, 1978), trace gases from various ice cores (Schmidt et al., 2012; Meinshausen et al., 2011), volcanic aerosols (Crowley et al., 2008), solar irradiance (Delaygue and Bard, 2009; Wang et al., 2005), sulphate aerosols (Lamarque et al., 2010) and land use (Pongratz et al., 2008; Hurtt et al., 2011). The warming from black carbon and the indirect effect of ozone, and the cooling from the indirect effect of sulphate aerosols were not included. Forcing data from PMIP3 and CMIP5 were concatenated or linearly blended before 1850 when necessary. From 1850 to 2005, all specified forcings are identical to the historical portion of the Representative Concentration Pathway (RCP) scenarios. See Appendix B for details on the implementation of the forcing protocol and how this may differ between models. All years in this paper are given as Common Era (CE) unless stated otherwise.

Diagnosed model equivalent radiative forcing estimates, for the various specified external forcings, are shown in Fig. 1. Given the large diversity of EMICs, not all models are able to apply the specified forcing in the same way. Some diagnosed estimates of equivalent radiative forcing are only approximate. This is especially true for sulphate aerosol and land-use forcing, which are more complex to implement and diagnose than most of the other externally specified forcings. The multi-model mean radiative forcing estimates for the direct effect of trace gases, sulphates and land-use change are very similar to estimates from the Task Group: RCP Concentrations Calculation and Data (Meinshausen et al., 2011), and present-day estimates are similar to those given in the AR4 (Forster et al., 2007). The ranges in diagnosed radiative forcing in Fig. 1 are also similar to the ranges from the models described by Fernández-Donado et al. (2012), with most of the variation between models due to the implementation of anthropogenic forcing (which includes aerosols and land-use change).

Models that participated in the historical last millennium simulations (B3, C2, C3, DC, GE, IA, I2, LO, ME, MI, UM, UV) used steady forcing to create the initial equilibrium state. Most models started from a steady state using forcing

Table 1. Summary of the primary components of the EMICs that participated in this intercomparison.

Model	Atmosphere[a]	Ocean[b]	Sea Ice[c]	Coupling[d]	Land Surface[e]	Biosphere[f]	Ice Sheets[g]	Sediment and weathering[h]
B3: Bern3D-LPJ (Ritz et al., 2011)	EMBM, 2-D(φ, λ), NCL, 10° × (3–19)°	FG with parameterized zonal pressure gradient, 3-D, RL, ISO, MESO, 10° × (3–19)°, L32 (Müller et al., 2006)	0-LT, DOC, 2-LIT	PM, NH, RW	Bern3D: 1-LST, NSM, RIV LPJ: 8-LST, CSM with uncoupled hydrology (Wania et al., 2009a,b)	BO (Parekh et al., 2008; Tschumi et al., 2008; Gangstø et al., 2011), BT (Sitch et al., 2003; Strassmann et al., 2008; Stocker et al., 2011), BV (Sitch et al., 2003)	N/A	CS, SW (Tschumi et al., 2011)
C2: CLIMBER-2.4 (Petoukhov et al., 2000)	SD, 3-D, CRAD, ICL, 10° × 51°, L10	FG, 2-D(φ, z), RL, 2.5°, L21 (Wright and Stocker, 1992)	1-LT, PD, 2-LIT	NM, NH, NW	1-LST, CSM, RIV	BO, BT, BV (Brovkin et al., 2002)	TM, 3-D, 0.75° × 1.5°, L20 (Calov et al., 2002)	N/A
C3: CLIMBER-3α (Montoya et al., 2006)	SD, 3-D, CRAD, ICL, 7.5° × 22.5°, L10 (Petoukhov et al., 2000)	PE, 3-D, FS, ISO, MESO, TCS, DC, 3.75° × 3.75°, L24	2-LT, R, 2-LIT (Fichefet and Morales Maqueda, 1997)	AM, NH, RW	1-LST, CSM, RIV (Pethoukhov et al., 2000)	BO (Six and Maier-Reimer, 1996), BT, BV (Brovkin et al., 2002)	N/A	N/A
DC: DCESS (Shaffer et al., 2008)	EMBM, 2-box in φ, LRAD, CHEM	2-box in φ, parameterized circulation and exchange, MESO, L55	Parameterized from surface temperature	NH, NW	NST, NSM	BO, BT	N/A	CS, CW
FA: FAMOUS XDBUA (Smith et al., 2012)	PE, 3-D, CRAD, ICL, 5° × 7.5°, L11 (Pope et al., 2000)	PE, 3-D, RL, ISO, MESO, 2.5° × 3.75°, L20 (Gordon et al., 2000)	0-LT, DOC, 2-LIT	NM, NH, NW	4-LST, CSM, RIV (Cox et al., 1999)	BO (Palmer and Totterdell, 2001)	N/A	N/A
GE: GENIE (Holden et al., 2013)	EMBM, 2-D(φ, λ), NCL, 10° × (3–19)° (Marsh et al., 2011)	FG, 3-D, RL, ISO, MESO, 10° × (3–19)°, L16 (Marsh et al., 2011)	0-LT, DOC, 2-LIT (Marsh et al., 2011)	PM, NH, RW (Marsh et al., 2011)	1-LST, BSM, RIV (Williamson et al., 2006)	BO, BT (Ridgwell et al., 2007; Williamson et al., 2006)	N/A	CS, SW (Ridgwell and Hargreaves, 2007)
IA: IAP RAS CM (Eliseev and Mokhov, 2011)	SD, 3-D, CRAD, ICL, 4.5° × 6°, L8 (Petoukhov et al., 1998)	PE, 3-D, RL, ISO, TCS, 3.5° × 3.5°, L32 (Muryshev et al., 2009)	0-LT, 2-LIT (Muryshev et al., 2009)	NM, NH, NW (Muryshev et al., 2009)	240-LST, CSM (Arzhanov et al., 2008)	BT	N/A	N/A
I2: IGSM 2.2 (Sokolov et al., 2005)	SD, 2-D(φ, Z), ICL, CHEM, 4° × 360°, L11 (Sokolov and Stone, 1998)	Q flux mixed-layer, anomaly diffusing, 4° × 5°, L11 (Hansen et al., 1984)	2-LT, (Hansen et al., 1984)	Q flux	CSM (Oleson et al., 2008)	BO (Holian et al., 2001), BT (Melillo et al., 1993; Felzer et al., 2004; Liu, 1996)	N/A	N/A
LO: LOVECLIM1.2 (Goosse et al., 2010)	QG, 3-D, LRAD, NCL, 5.6° × 5.6°, L3 (Opsteegh et al., 1998)	PE, 3-D, FS, ISO, MESO, TCS, DC, 3° × 3°, L30 (Goosse and Fichefet, 1999)	3-LT, R, 2-LIT (Fichefet and Morales Maqueda, 1997)	NM, NH, RW (Goosse et al., 2010)	1-LST, BSM, RIV	BO (Mouchet and François, 1996), BT, BV (Brovkin et al., 2002)	TM, 3-D, 10 km × 10 km, L30 (Huybrechts, 2002)	N/A
ME: MESMO 1.0 (Matsumoto et al., 2008)	EMBM, 2-D (φ, λ), NCL, 10° × (3–19)° (Fanning and Weaver, 1996)	FG, 3-D, RL, ISO, MESO, 10° × (3–19)°, L16 (Edwards and Marsh, 2005)	0-LT, DOC, 2-LIT (Edwards and Marsh, 2005)	PM, NH, RW	NST, NSM, RIV (Edwards and Marsh, 2005)	BO	N/A	N/A

Table 1. Continued.

Model	Atmosphere[a]	Ocean[b]	Sea Ice[c]	Coupling[d]	Land Surface[e]	Biosphere[f]	Ice Sheets[g]	Sediment and weathering[h]
MI: MIROC-lite (Oka et al., 2011)	EMBM, 2-D(φ, λ), NCL, 4° × 4°	PE, 3-D, FS, ISO, L35, MESO, TCS, 4 ° × 4° (Hasumi, 2006)	0-LT, R, 2-LIT (Hasumi, 2006)	PM, NH, NW	1-LST, BSM	N/A	N/A	N/A
ML: MIROC-lite-LCM (Tachiiri et al., 2010)	EMBM, 2-D(φ, λ), NCL, 6° × 6° (Oka et al., 2011), tuned for 3 K ECS	PE, 3-D, FS, ISO, MESO, TCS, 6° × 6°, L15 (Hasumi, 2006)	0-LT, R, 2-LIT (Hasumi, 2006)	NM, NH (Oka et al., 2011), RW	1-LST, BSM (Oka et al., 2011)	BO (Palmer and Totterdell, 2001), loosely coupled BT (Ito and Oikawa, 2002)	N/A	N/A
SP: SPEEDO V2.0 (Severijns and Hazeleger, 2010)	PE, 3D, LRAD, ICL, T30, L8 (Molteni, 2003)	PE, 3D, FS, ISO, MESO, TCS, DC, 3 × 3, L20 (Goosse and Fichefet, 1999)	3-LT, R, 2-LIT (Fichefet and Morales Maqueda, 1997)	NM, NH, NW (Cimatoribus et al., 2012)	1-LST, BSM , RIV (Opsteegh et al., 1998)	N/A	N/A	N/A
UM: UMD 2.0 (Zeng et al., 2004)	QG, 3-D, LRAD, ICL, 3.75° × 5.625°, L2 (Neelin and Zeng, 2000; Zeng et al., 2000)	Q flux mixed-layer, 2-D surface (Hansen et al., 1984), deep ocean box model, 3.75° × 5.625°	N/A	Energy and water exchange only	2-LST with 2-layer soil moisture (Zeng et al., 2000)	BO (Archer et al., 2000), BT, BV (Zeng, 2003; Zeng et al., 2005)	N/A	N/A
UV: UVic 2.9 (Weaver et al., 2001)	DEMBM, 2-D (φ, λ), NCL, 1.8° × 3.6°	PE, 3-D, RL, ISO, MESO, 1.8° × 3.6°, L19	0-LT, R, 2-LIT	AM, NH, NW	1-LST, CSM, RIV (Meissner et al., 2003)	BO (Schmittner et al., 2008), BT, BV (Cox, 2001)	TM, 3-D, 20 km × 20 km, L10 (Fyke et al., 2011)	CS, SW (Eby et al., 2009)

[a] EMBM = energy moisture balance model; DEMBM = energy moisture balance model including some dynamics; SD = statistical–dynamical model; QG = quasi-geostrophic model; 2-D(φ, λ) = vertically averaged; 3-D = three-dimensional; LRAD = linearized radiation scheme; CRAD = comprehensive radiation scheme; NCL = non-interactive cloudiness; ICL = interactive cloudiness; CHEM = chemistry module; $n° \times m° = n$ degrees latitude by m degrees longitude horizontal resolution; Lp = p vertical levels.

[b] FG = frictional geostrophic model; PE = primitive equation model; 2-D(φ, z) = zonally averaged; 3-D = three-dimensional; RL = rigid lid; FS = free surface; ISO = isopycnal diffusion; MESO = parameterization of the effect of mesoscale eddies on tracer distribution; TCS = complex turbulence closure scheme; DC = parameterization of density-driven downward-sloping currents; $n° \times m° = n$ degrees latitude by m degrees longitude horizontal resolution; Lp = p vertical levels.

[c] n-LT = n layer thermodynamic scheme; PD = prescribed drift; DOC = drift with oceanic currents; R = viscous-plastic or elastic-viscous-plastic rheology; 2-LIT = two-level ice thickness distribution (level ice and leads).

[d] PM = prescribed momentum flux; AM = momentum flux anomalies relative to the control run are computed and added to climatological data; NM = no momentum flux adjustment; NH = no heat flux adjustment; RW = regional freshwater flux adjustment; NW = no freshwater flux adjustment.

[e] NST = no explicit computation of soil temperature; n-LST = n layer soil temperature scheme; NSM = no moisture storage in soil; BSM = bucket model for soil moisture; CSM = complex model for soil moisture; RIV = river routing scheme.

[f] BO = model of oceanic carbon dynamics; BT = model of terrestrial carbon dynamics; BV = dynamical vegetation model.

[g] TM = thermomechanical model; 3-D = three-dimensional; $n° \times m° = n$ degrees latitude by m degrees longitude horizontal resolution; n km × m km = horizontal resolution in kilometres; Lp = p vertical levels.

[h] CS = complex ocean sediment model; SW = simple, specified or diagnostic weathering model, CW = complex, climate-dependent weathering.

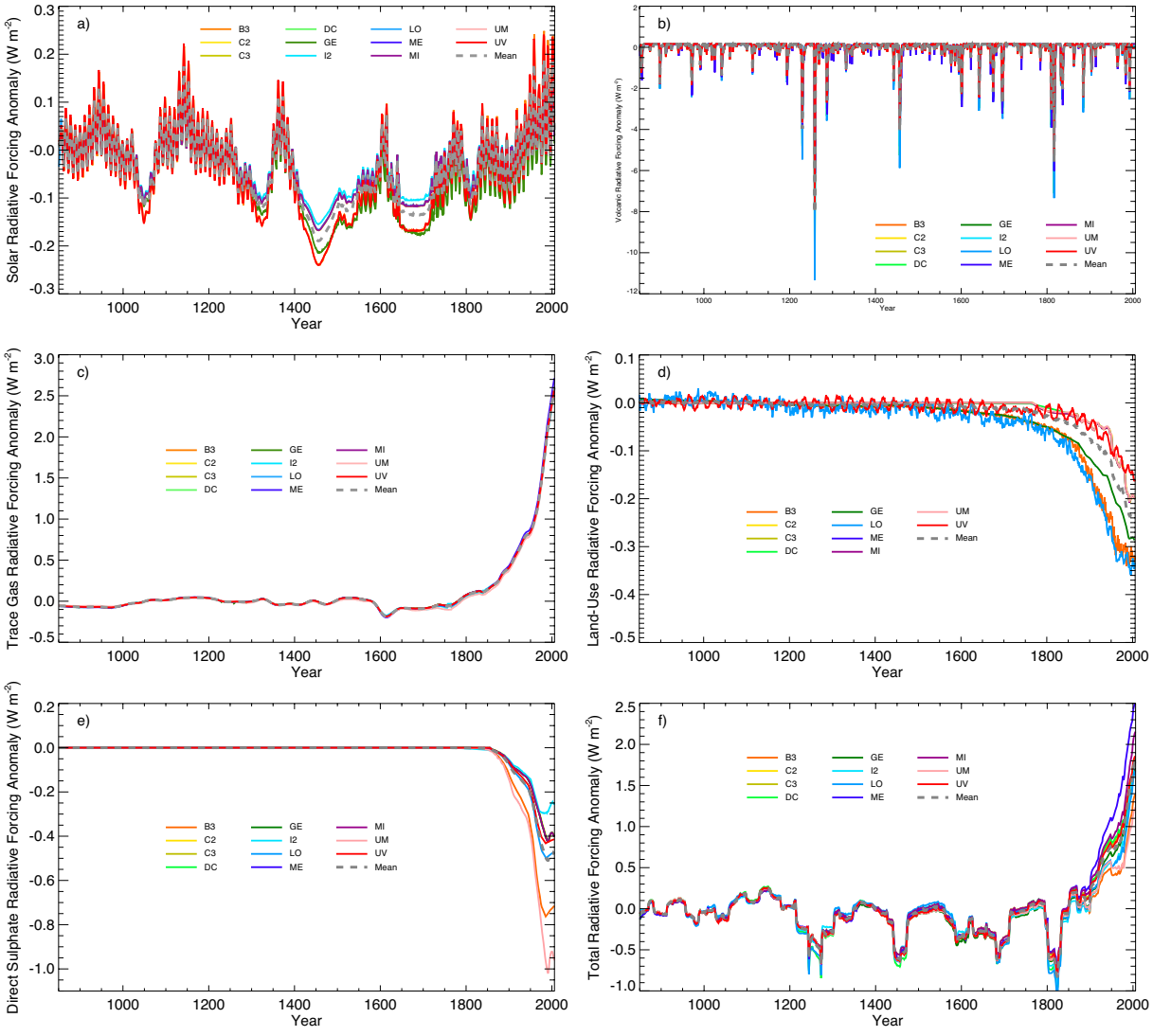

Fig. 1. Annual average radiative forcing estimates, from specified forcing changes in the historical simulations, for 11 of the participating models. Changes in radiative forcing from changes in solar irradiance are shown in **(a)**, volcanic aerosols in **(b)**, greenhouse gases in **(c)**, land use in **(d)**, the direct effect of sulphate aerosols in **(e)**, and all forcings in **(f)**. Due to the complexity of implementing forcing from land use and the direct effects of sulphate aerosols in some models, the diagnosed radiative forcing estimates should be considered to be only approximate. Models that specified equivalent task group radiative forcings may be exactly overplotted and appear to be missing (see Appendix B for details on forcing). Land-use radiative forcing was not available for model I2. Radiative forcing is plotted as an anomaly of the multi-model mean over the century centred at year 900. Forcing estimates in panels **(a)** to **(e)** are unfiltered while the results in **(f)** have been processed with a 30 yr moving average, rectangular filter. Changes in radiative forcing due to changes in orbit are much smaller than any of the other forcings and are not shown separately, but they are included in the total radiative forcing shown in **(f)**.

from the year 850, but the B3 model started from equilibrium at the Last Glacial Maximum in order to ensure that its permafrost and peatland components were in a consistent initial state by the year 850.

Models were then integrated to the year 2005 under various specified transient forcings. Nine historical simulations with specified CO_2 concentrations were performed. Seven simulations specified only one of the following transient forcings: non-CO_2 trace gases, CO_2, land use, solar luminosity, orbital parameters, sulphate aerosols or volcanic aerosols. The other two simulations specified either all or none of these forcing changes. The simulation with no changes in forcing is merely a continuation of the equilibrium simulation and can be considered a control experiment. The all-forcing simulation was used as the initial condition for future simulations in Zickfeld et al. (2013).

For models with complete carbon cycles (B3, DC, GE, I2, ME, UM and UV), three additional free CO_2 historical

simulations were performed. In these experiments, the initial conditions and forcings were the same as for the equivalent historical, specified CO_2 simulations, but CO_2 concentrations were no longer specified. In the equivalent "all" forcing experiment, changing anthropogenic CO_2 emissions were specified. In the equivalent "control", no anthropogenic CO_2 emissions were applied. The third simulation had changes only in natural forcings (orbital parameters, solar luminosity and volcanic aerosols) and no anthropogenic CO_2 emissions.

Several idealized experiments were also performed in order to calculate standard climate and carbon cycle metrics. All of these experiments were started from an equilibrium state with a CO_2 concentration near 280 ppm and integrated for 1000 yr. There were seven idealized experiments performed in total. Two experiments specified an instantaneous increase of CO_2 to a constant concentration at $2\times$ and $4\times$ the initial concentration. These were used to help assess equilibrium climate sensitivity. Another experiment specified an instantaneous increase to $4\times$ the initial CO_2 but then allowed CO_2 to evolve freely. This experiment was used to determine the time scales over which carbon perturbations are removed from the atmosphere.

The other four idealized experiments specified an increase in CO_2 at 1 % per year until reaching $4\times$ the initial CO_2 concentration. One experiment allowed CO_2 to freely evolve after reaching $4\times$ the initial concentration. This experiment was used to assess the models' carbon-climate response (CCR). This is calculated as the change in surface air temperature (SAT) divided by the total amount of accumulated emissions from some reference period (Matthews et al., 2009). For the other three experiments, which started with an increase in CO_2 at 1 % per year, CO_2 was fixed after reaching $4\times$ the initial concentration. These experiments were used to determine the models' carbon cycle feedbacks. One experiment was fully coupled, one excluded the changes in radiative forcing from increasing CO_2, and one excluded the direct effects of increasing CO_2 on land and ocean carbon fluxes. The CO_2 concentration–carbon sensitivity can be calculated directly as the change in land or ocean carbon, in the experiment that excludes the radiative forcing from increasing CO_2 (radiatively uncoupled), divided by the change in atmospheric CO_2. The climate–carbon sensitivity can be calculated directly as the change in land or ocean carbon, in the experiment that excludes the effects of increasing CO_2 on land and ocean carbon fluxes (biogeochemically uncoupled), divided by the change in SAT. The fully coupled simulation was also used to assess transient climate sensitivities, ocean heat uptake efficiency and zonal amplification. Ocean heat uptake efficiency is the global average heat flux divided by the change in SAT, and zonal temperature amplification is the zonal average SAT anomaly divided by the global average SAT anomaly.

3 Results and discussion

3.1 Historical climate response

There is a very large range in the absolute SAT simulated over the historical period by the models involved in this intercomparison. Absolute SAT is a difficult quantity to measure, but Jones et al. (1999) estimate the absolute global average value of SAT to be approximately 14 °C between the years 1960 and 1990. As seen in Fig. 2a, the annual average SAT at 850 varies from 12.3 to 17.2 °C. All of the models are using similar externally specified forcing, so this large range in initial conditions must be due to internal model differences. Most comparisons between models and observational datasets only examine anomalies from a particular reference period (as in Fig. 2b). However, the large differences between initial states might influence the models' responses to changing climate forcing. Some feedbacks, such as the albedo changes from reductions in snow or ice, and hence an individual model's climate sensitivity (Weaver et al., 2007), would likely depend on the models' initial state.

Although the average model trend over the 20th century (0.79 °C) is close to the observed trends (0.73 °C) (Morice et al., 2012), there is still considerable spread in model response (0.4 to 1.2 °C). One difficulty in comparing EMICs involves the large variation in complexity between models. The implementation of some of the forcing needs to be highly parameterized or even specified in many models. Aerosols and land-use change can be particularly challenging to implement. A few EMICs are not able to apply all of the forcings specified in the experimental design, which adds to the model spread.

For the specified external forcings over the 20th century, five models appear to stay mostly within the observational uncertainty envelope for this period, five tend to overestimate the observed trends, and two tend to underestimate the trends (Fig. 2b). The model with the largest trend (ME) did not include any sulphate aerosol forcing. Without the cooling associated with this forcing, the model would be expected to overestimate 20th century warming. On the other hand, the UM model, which simulates the 20th century trend well, includes estimates of the indirect effect of sulphate aerosols but not the countering ozone and black carbon forcing (see Appendix B). Given the large number of models included in this intercomparison, the variation in the application of external forcing appears to average out, and the model mean trend agrees well with observations.

It is unclear if there is a relationship between the pre-industrial climate state and the climate response over the 20th century. The two models with the strongest 20th century response also start from the coldest initial state. The model with the weakest response starts from the second warmest state. Using all models, the linear correlation (r) between initial state and 20th century warming is about 0.4. If the two models with the strongest and the model with the weakest response are excluded, there is no clear relationship ($r = 0.2$).

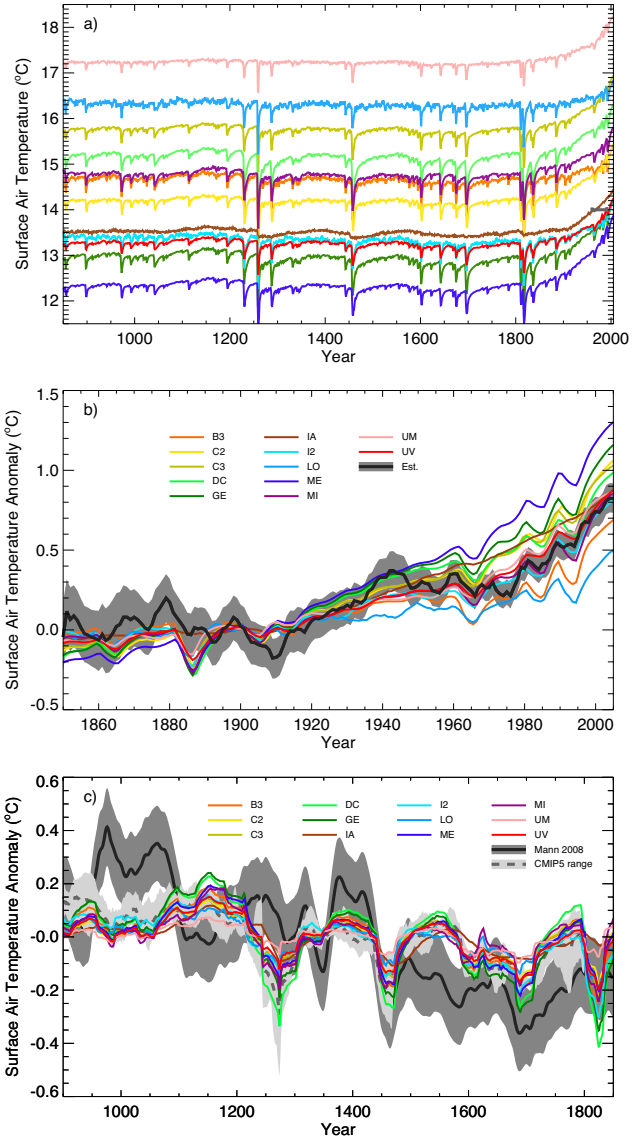

Fig. 2. Global surface air temperature from the historical all-forcing simulation for 12 of the participating models. Absolute temperatures are shown for the entire simulation in **(a)**. The small dark grey bar at 14 °C between 1960 and 1990 is an estimate of the average absolute surface air temperature from Jones et al. (1999) over this period. Temperature anomalies from 1850 are shown in **(b)**. The dark grey line shows changes in SAT, and the grey shading indicates the uncertainty, from Morice et al. (2012). The model results and the data estimates are shown as anomalies from the average over the decade centred at year 1900 and have been processed with a 5 yr moving average, rectangular filter. Temperature anomalies before 1850 are shown in **(c)**. The dark grey line shows changes in global SAT, and the grey shading indicates the uncertainty, from the error-in-variables (EIV) reconstruction of Mann et al. (2008). The grey dashed line shows the model mean, and the light grey shading the model range, of the CMIP5 models that carried out the PMIP3 "last millennium" experiment. The model results and the data estimates are shown as anomalies from the average over the entire period (900 to 1850 or 900 to 1800 for the CMIP5 models) and have been processed with a 30 yr moving average, rectangular filter.

Given that many factors other than initial state influence a model's 20th century climate response, a strong relationship is not expected.

Over the pre-industrial period (Fig. 2c), the models tend to show a relatively weak response compared to the Mann et al. (2008) global SAT reconstruction. The reconstruction indicates a relatively warm period near year 1000 (often called the Medieval Climate Anomaly, or MCA) and a cooler period near year 1700 (often referred to as the Little Ice Age, or LIA). In terms of anomalies from today, it is mostly the MCA that is not well reproduced by the models since they agree reasonably well with the reconstructed difference in temperature between the LIA and present climate ($\sim 1\,^{\circ}\mathrm{C}$).

It does appear that, on average, the models show a stronger cooling response to several large volcanic eruptions than is indicated by the reconstructions (see eruptions near years 1280 and 1810 in Fig. 2). Given that volcanic forcing is generally short-lived, it is difficult to determine if the strong cooling response is due to excessive volcanic forcing or a lack of temporal resolution in the SAT reconstruction. It is also possible some of the proxies used in the reconstructions are not very sensitive to volcanic cooling (Mann et al., 2012). Temperature reconstructions over the last millennium (as in Mann et al., 2008 or Frank et al., 2010) tend to show little agreement.

Several CMIP5 models have also carried out the PMIP3 "last millennium" or CMIP5 "past1000" experiment (bcc-csm1-1, CCSM4, FGOALS-gl, GISS-E2-R, IPSL-CM5A-LR, MIROC-ESM, MPI-ESM-P), and these results are available through the CMIP5 data portal. The range and mean of these CMIP5 model simulations are also shown in Fig. 2c. The mean response of the CMIP5 models is very similar to the mean EMIC response, including a strong SAT response to volcanic forcing. This is perhaps expected since both sets of models are following the same PMIP3 external forcing protocol. A similar strong response to volcanic forcing is also seen in Fernández-Donado et al. (2012). Given the low levels of internal variability in EMICs, the range in the EMIC's SAT response is mostly contained within the CMIP5 model range. This weakly forced response between the MCA and LIA, found here in both EMICs and CMIP5 models, is also seen in several other modelling studies – especially for models that specify weak solar irradiance variation between these periods (Goosse et al., 2010; Jungclaus et al., 2010; Servonnat et al., 2010; Fernández-Donado et al., 2012). However, Feulner (2011) finds good agreement with Northern Hemisphere temperature reconstructions for a solar constant of $1361\,\mathrm{W\,m^{-2}}$, weak solar variations and the Crowley (2000) volcanic forcing.

The amount of heat taken up by the ocean is an important factor in determining transient climate response and sea level change. The models' changes in ocean heat content over the 20th century are shown in Fig. 3a. While the data estimates are only to 2000 m depth and the model heat content change shown is over the entire ocean depth, it appears

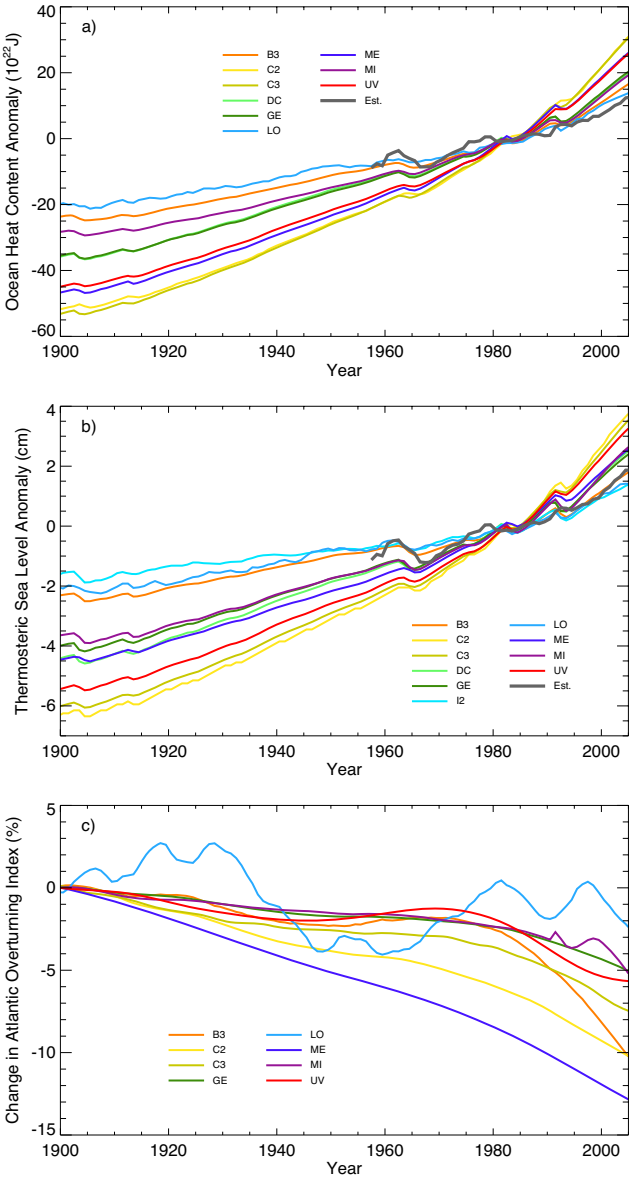

Fig. 3. Changes in global ocean heat content **(a)**, thermosteric sea level rise **(b)**, and North Atlantic overturning index **(c)** over the last century. The dark grey lines are estimates of the change in heat content **(a)**, and the thermosteric component of sea level change **(b)**, of the first 2000 m of the ocean, from Levitus et al. (2012). Ocean heat content **(a)** and thermosteric sea level **(b)** are plotted as anomalies from the year 1957 to 2005 average. Note that the model heat content and sea level changes are averages over the entire ocean so these would be expected to be somewhat larger than the values estimated over the first 2000 m. The North Atlantic overturning index **(c)** is shown as a percent change from the decade centred at year 1900 and was processed with a 30 yr moving average, rectangular filter.

that many models may be overestimating ocean heat uptake. Some of the modelled differences from observations could be due to too much or too little surface warming. The two models that agree well with ocean heat uptake estimates are the same models that slightly underestimate atmospheric surface warming over the 20th century. Estimates of past thermosteric sea level rise (Fig. 3b) show similar differences between the models' and data estimates, with the models generally simulating more thermosteric sea level rise than observed. This is not surprising since the largest component of thermosteric sea level changes is from changes in ocean heat content.

The response of the thermohaline circulation in the Atlantic, as indicated by a simple Atlantic meridional overturning index (defined as the maximum value of the overturning stream function in the North Atlantic), indicates a moderate slowing in all models (between about 0.8 and 2.1 Sv, or from 3 to 13 %). Direct measurements of the thermohaline circulation are difficult, and trends are hard to distinguish from natural variability. There is, therefore, still some controversy as to the response of the meridional overturning circulation over the 20th century (Latif et al., 2006). However, this moderate response to a warming climate is similar to what has been seen in previous studies (Plattner et al., 2008).

3.2 Idealized climate response metrics

In order to assess the models' responses in a more controlled environment, several standard idealized experiments were performed. Idealized experiments with CO_2 increasing at a rate of 1 % per year until reaching two or four times the initial level of pre-industrial CO_2 were used to assess the transient climate response and equilibrium climate sensitivities. Here we define the equilibrium climate sensitivity to be the change in SAT after 1000 yr, even though the models are not truly in equilibrium. There is a relatively large range in the equilibrium climate sensitivity (see Fig. 4a and Table 2). Equilibrium climate sensitivity at $2 \times CO_2$ ranges between 1.9 and 4.0 °C, and at $4 \times CO_2$ between 3.5 and 8.0 °C. For comparison, the range of $2 \times CO_2$ equilibrium climate sensitivity for CMIP3 models is 2.1 to 4.4 °C, and the range for CMIP5 models is estimated to be 2.1 to 4.7 °C (Andrews et al., 2012). The ocean heat uptake efficiency was also calculated from this $4 \times CO_2$ idealized experiment, and it is interesting to note that the model with the highest uptake efficiency (LO) is also one of the models with the lowest ocean heat uptake over the 20th century. This implies that the lower than average (but closer to observed) heat uptake is most likely due to the model's lower than average 20th century warming. This may not be the case with B3, which also has lower than average 20th century ocean heat uptake, but shows one of the lowest heat uptake efficiencies.

Figure 4b shows the models' zonal SAT amplification, which is calculated as the zonal SAT change divided by the global mean change at year 140 of the 1 % increase to

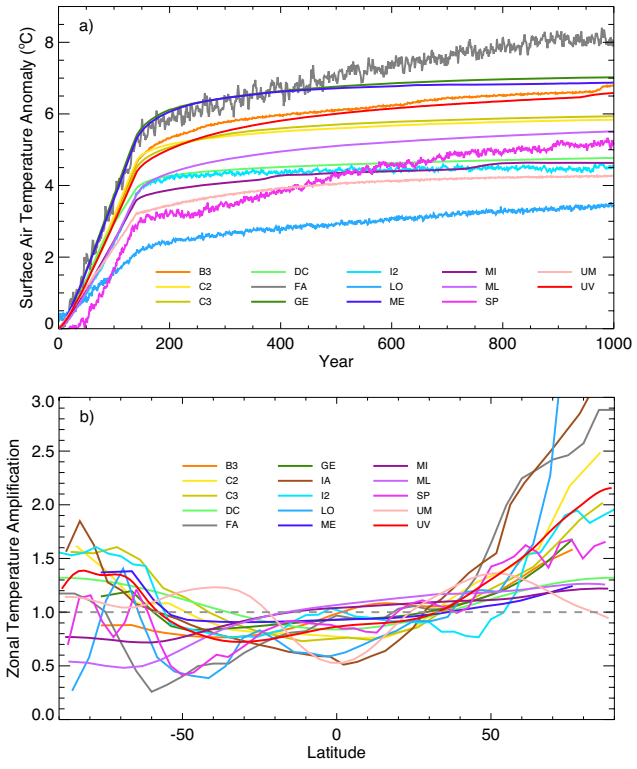

Fig. 4. Surface air temperature **(a)** and zonal temperature amplification **(b)** for all 15 participating models, from a 1 % increase to $4 \times CO_2$ simulation. The zonal temperature amplification is calculated as the zonal anomaly divided by the global average anomaly at year 140, which roughly corresponds to the time of CO_2 quadrupling.

$4 \times CO_2$ experiment. The temperature amplification at year 70 (when $2 \times CO_2$ is reached, not shown) is similar. Some models (DC, ME, MI, ML) exhibit very little polar amplification, showing a nearly flat zonal response. Two models (IA and LO) show polar amplification in the north to be larger than 3.0. Although the model with the highest polar amplification has one of the lowest climate sensitivities, and starts from one of the warmest initial states, there appears to be no simple relationship between polar amplification, climate sensitivity and initial state.

3.3 Historical carbon-cycle response

The ability to reproduce trends in the carbon cycle is another important requirement for models that are used to predict the fate of anthropogenic carbon. For the historical all-forcing experiment (as for RCPs), CO_2 concentrations are specified, but models with a complete carbon cycle can still calculate emissions that are compatible with the specified CO_2. The overall average EMIC carbon cycle response for the 1990s is within the uncertainty range of estimated values, except for diagnosed emissions, which are slightly underestimated (see Table 3). The EMIC mean in Table 3 excludes the two models (ME, UM) that do not transfer carbon with land-use change. These models would be expected to overestimate diagnosed emissions due to the lack of emissions from land-use change. This can be seen in the accumulated fluxes from 1800–2000, where they underestimate land fluxes to the atmosphere, and thus overestimate total diagnosed emissions by 61 to 103 Pg of carbon.

The fluxes of carbon to the atmosphere are shown in Fig. 5a. All models reproduce the estimated fluxes to the ocean within the uncertainty ranges, between 1980 and 2005. Although all models remain within the large range of uncertainty for land fluxes in the 1980s, many appear to underestimate recent land fluxes, especially since 2000. A few models are able to reproduce trends in emissions reasonably well, but most underestimate recent emissions, apparently because of insufficient net uptake on land.

Figure 5b shows the accumulated fluxes of carbon since 1800. The integral changes in pools (or emissions) are also shown with associated uncertainty as cross bars at 1994 (estimates from Sabine et al., 2004). Again, all models estimate total ocean uptake within the range of uncertainty (see Table 3). Total land pool changes are much more variable, with only half of the models estimating fluxes within the range of uncertainty. However, most models do remarkably well at estimating total emissions between 1800 and 1994. Two models overestimate total emissions, and one underestimates emissions.

Figure 5c breaks down the land fluxes into two components. The land-use change (LUC) flux component is estimated from a simulation with only land-use change forcing. The residual flux is the total flux from an all-forcing simulation minus the LUC component. As in Houghton (2008), the LUC component should not include any interaction between land-use change and changes in climate or CO_2. Any interaction terms are part of the residual flux. As expected, the UM model, which does not directly include carbon transfer as part of the model's land-use forcing, shows near-zero LUC carbon fluxes. If the diagnosed LUC flux is correct, then most other models also appear to underestimate carbon fluxes to the atmosphere from LUC. Most models also tend to underestimate residual land uptake.

It would appear that any underestimation of LUC and the residual flux partially cancel, allowing some models to generate reasonable overall land fluxes. If LUC fluxes were higher, then the residual uptake by land would need to be greater. In general, it would appear that all models are either overestimating the response of the land carbon cycle to climate change or not taking up sufficient carbon through fertilization of vegetation (either from CO_2 or deposition of N). Only the I2 model includes an interactive land nitrogen cycle, which incorporates nitrogen limitation of photosynthesis. None of the models include anthropogenic nitrogen deposition as part of their vegetation component forcing. There is a great deal of uncertainty in future vegetation response, but even the

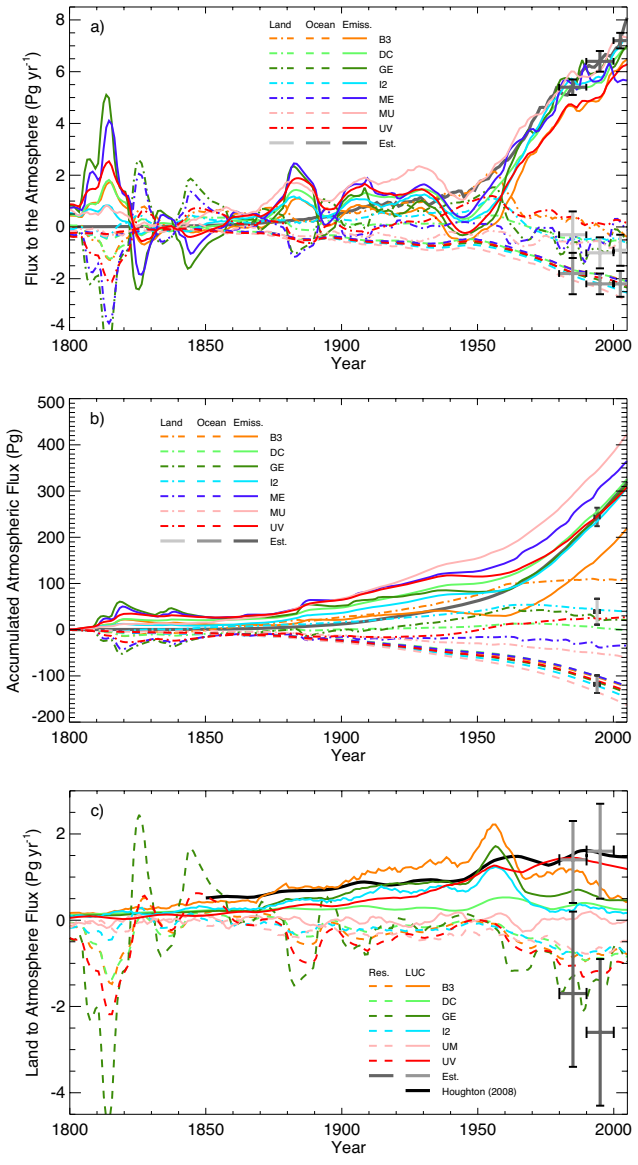

Fig. 5. Carbon fluxes to the atmosphere from the land, ocean and anthropogenic emissions since 1800 from models with land and ocean carbon cycle components. Fluxes are shown in **(a)**, the accumulated flux or change in pool carbon in **(b)** and the components of the land flux in **(c)**. The land-use change (LUC) component was calculated from a simulation that only included land-use change forcing. The residual component (Res.) is calculated as the difference in land fluxes between a simulation with all forcing and one with just land-use change forcing. The model results in **(a)** and **(c)** have been processed with a 10 yr moving average, rectangular filter. The data and uncertainty estimates for the years 1980–1989, 1990–1999 and 2000–2005 in **(a)** and **(c)** are from Table 1 in Denman et al. (2007). The data and uncertainty estimates at year 1994 in **(b)** are from Sabine et al. (2004). The solid black line in **(b)** indicates fossil fuel emission estimates from Boden et al. (2012) and in **(c)** the LUC flux estimates from Houghton (2008).

current response does not appear to be well simulated by most models.

It is possible that the diagnosed partitioning between the LUC and residual flux is poorly estimated by the LUC only forcing simulation – at least in terms of the definition of Houghton (2008). There may be a small feedback on the carbon cycle due to the cooling from local albedo changes. Additional simulations with GENIE (not shown) indicate that there is likely some underestimation of LUC fluxes in the simulation with only land-use forcing due to the climate–carbon feedback on soil respiration. The cooling from the albedo change reduces soil respiration, which in turn reduces the apparent LUC flux. Simulations with fixed albedo (and thus climate) indicate that this underestimation may be significant. Further investigation is required to determine if this small feedback leads to a significant underestimation of the LUC flux in other models.

3.4 Idealized carbon-cycle response metrics

Standard carbon cycle metrics are also calculated from specified 1 % increasing to $4 \times CO_2$ experiments. In addition to the standard fully coupled experiment, two additional partially coupled experiments were done by EMICs with a complete carbon cycle. One experiment excluded only the direct greenhouse radiative effects of increasing CO_2 (radiatively uncoupled) while the other experiment excluded only the direct effects of increasing CO_2 on land and ocean carbon fluxes (biogeochemically uncoupled). For specified CO_2 experiments, the CO_2 concentration–carbon sensitivity (β) can be calculated directly as the change in land or ocean carbon divided by the change in atmospheric CO_2 in a radiatively uncoupled simulation. The climate–carbon sensitivity (γ) is calculated directly as the change in land or ocean carbon divided by the change in SAT in a biogeochemically uncoupled simulation.

These parameters are calculated differently from the C^{4}MIP intercomparison project (Friedlingstein et al., 2006) due to the specification of CO_2 concentrations rather than emissions, which results in somewhat lower estimates of γ (Plattner et al., 2008; Gregory et al., 2009; Zickfeld et al., 2011). Carbon cycle sensitivities can also be calculated indirectly from the difference between a fully coupled simulation and either a biogeochemically uncoupled simulation (for γ) or a radiatively uncoupled simulation (for β). The value of γ, and to a lesser extent β, is highly dependent on the method of calculation for models with large nonlinear climate and CO_2 interactions (Zickfeld et al., 2011). Plattner et al. (2008) calculated β directly and γ indirectly.

Directly calculated sensitivities at year 140 (and year 995) are shown in Table 4, and Fig. 6 shows how these sensitivities change through time. The CO_2 concentration–carbon sensitivities for land (β_L) are relatively constant after 140 yr (CO_2 quadrupling) for most models. This is similar for γ_L, except for the B3 model and, to a lesser extent, the UM model. The

Table 2. Standard metrics that help characterize model response. T_{PI} is the average surface air temperature between 850 and 1750, and ΔT_{20th} is the change in surface air temperature over the 20th century, both from the historical "all" forcing experiment. TCR_{2X}, TCR_{4X}, and ECS_{4X} are the changes in global average model surface air temperature from the decades centred at years 70, 140, and 995 respectively, from the idealized 1 % increase to $4 \times CO_2$ experiment. The ocean heat uptake efficiency, κ_{4X}, is calculated from the global average heat flux divided by TCR_{4X} for the decade centred at year 140, from the same idealized experiment. Note that ECS_{2x} was calculated from the decade centred at about year 995 from a $2 \times CO_2$ pulse experiment.

Model	T_{PI} (°C)	ΔT_{20th} (°C)	TCR_{2X} (°C)	ECS_{2x} (°C)	TCR_{4X} (°C)	ECS_{4X} (°C)	κ_{4X} ($W\,m^{-2}\,C^{-1}$)
B3	14.6	0.57	2.0	3.3	4.6	6.8	0.58
C2	14.2	0.91	2.1	3.0	4.7	5.8	0.84
C3	15.7	0.91	1.9	3.2	4.5	5.9	0.93
DC	15.1	0.84	2.1	2.8	3.9	4.8	0.72
FA	–	–	2.3	3.5	5.2	8.0	0.55
GE	12.9	1.00	2.5	4.0	5.4	7.0	0.51
IA	13.5	0.80	1.6	–	3.7	4.3	–
I2	13.3	0.70	1.5	1.9	3.7	4.5	–
LO	16.3	0.38	1.2	2.0	2.1	3.5	1.17
ME	12.3	1.15	2.4	3.7	5.3	6.9	0.55
MI	14.7	0.71	1.6	2.4	3.6	4.6	0.66
ML	–	–	1.6	2.8	3.7	5.5	1.00
SP	–	–	0.8	3.6	2.9	5.2	0.84
UM	17.2	0.79	1.6	2.2	3.2	4.3	–
UV	13.2	0.75	1.9	3.5	4.3	6.6	0.92
EMIC mean	14.8	0.78	1.8	3.0	4.0	5.6	0.8
EMIC range	12.3 to17.5	0.38 to 1.15	0.8 to 2.5	1.9 to 4.0	2.1 to 5.4	3.5 to 8.0	0.5 to 1.2

Table 3. Average carbon fluxes to the atmosphere over the 1990s and accumulated carbon fluxes from 1800 to 1994. $Land_{LUC}$ is an estimate of land-use change fluxes from simulations with only land-use forcing. $Land_{Res}$ is the residual land flux, which is derived from the land flux from a simulation with all forcing minus $Land_{LUC}$. All other model fluxes are from differences between the all-forcing and control simulations. Estimates of average fluxes are from Table 7.1 of Denman et al. (2007), and estimates of accumulated fluxes are from Table 1 of Sabine et al. (2004). The change in atmospheric carbon storage between 1800 and 1994 is estimated to be 164 ± 4 Pg in Sabine et al. (2004). Although the change in CO_2 between 1800 and 1994 was specified to be 75 ppm in the all-forcing simulations, due to different estimates of atmospheric volume, the change in atmospheric carbon storage in the models is between 158 and 165 Pg.

	Average carbon flux: 1990 to 1999 ($Pg\,yr^{-1}$)				Accumulated flux: 1800 to 1994 (Pg)		
Model	$Land_{LUC}$	$Land_{Res}$	Ocean	Emissions	Land	Ocean	Emissions
B3	0.7	−0.8	−1.8	5.2	108	−104	167
DC	0.3	−0.9	−1.8	5.7	4	−102	260
GE	0.5	−1.4	−2.1	6.1	21	−114	251
I2	0.3	−0.7	−2.2	5.9	43	−122	237
ME*		−0.6	−1.9	5.9	−38	−102	305
UM*		−0.6	−2.4	6.2	−51	−136	344
UV	1.3	−1.2	−2.0	5.2	24	−112	251
EMIC mean*	0.6	−1.0	−2.0	5.6	40	−111	233
EMIC range*	0.3 to 1.3	−1.4 to −0.7	−2.2 to −1.8	5.2 to 6.1	4 to 108	−122 to −102	167 to 260
Estimates	1.6	−2.6	−2.2	6.4	39	−118	244
Uncertainty	0.5 to 2.7	−4.3 to −0.9	−2.6 to −1.8	6.0 to 6.8	11 to 67	−137 to −99	224 to 264

* The ME and UM models were excluded from the EMIC model mean and range calculations, because they did not include any direct carbon exchange due to changes in land use. Only the total land flux is reported for these models.

Table 4. Carbon cycle sensitivities and metrics from idealized 4 $\times CO_2$ experiments. β_L (or β_O) is the change in land (or ocean) carbon divided by the change in atmospheric CO_2 in a radiatively uncoupled simulation. γ_L (or γ_O) is the change in land (or ocean) carbon divided by the change in atmospheric temperature, in a biogeochemically uncoupled simulation. CCR is the carbon-climate response and is calculated as atmospheric temperature change divided by diagnosed emissions (Matthews et al., 2009). β_L, γ_L, β_O, γ_O, and CCR are all averages over the decade centred at about year 140 from a 1 % increase to $4 \times CO_2$ experiment. Numbers in parentheses are averages over the decade centred at year 995. $Yr50_{4X}$ is the year that emissions remaining in the atmosphere fall below 50 %, from an instantaneous $4 \times CO_2$ pulse experiment.

Model	β_L (Pg ppm^{-1})	γ_L (Pg C^{-1})	β_O (Pg ppm^{-1})	γ_O (Pg C^{-1})	CCR (C Eg^{-1})	$Yr50_{4X}$ (yr)
B3	0.85 (1.47)	−67.5 (−179.8)	0.77 (3.07)	−6.4 (−24.9)	1.77 (2.02)	248
DC	0.76 (1.35)	−56.1 (−94.1)	0.78 (3.26)	−8.3 (−57.1)	1.42 (1.20)	112
GE	1.04 (1.34)	−78.0 (−78.0)	0.99 (3.86)	−0.1 (−35.8)	1.94 (1.65)	124
I2	0.22 (0.24)	−29.7 (−37.5)	1.04 (3.13)	−15.0 (−66.4)	1.37 (1.08)	84
ME	0.67 (0.75)	−75.5 (−71.2)	0.83 (2.90)	−9.6 (−55.9)	2.12 (1.94)	284
ML	0.57 (0.57)	−96.9 (−115.8)	0.86 (2.86)	−6.9 (−22.6)	1.38 (1.43)	60
UM	0.32 (0.48)	−6.9 (−41.0)	1.32 (3.90)	−22.9 (−111.5)	1.07 (0.92)	64
UV	1.09 (1.43)	−81.6 (−72.7)	0.82 (2.69)	−7.8 (−91.6)	1.48 (1.81)	60
EMIC mean	0.69 (0.95)	−61.5 (−86.3)	0.92 (3.21)	−9.6 (−58.2)	1.57 (1.51)	130
EMIC range	0.22 to 1.09	−96.9 to −6.9	0.77 to 1.32	−22.9 to −0.1	1.07 to 2.12	60 to 284

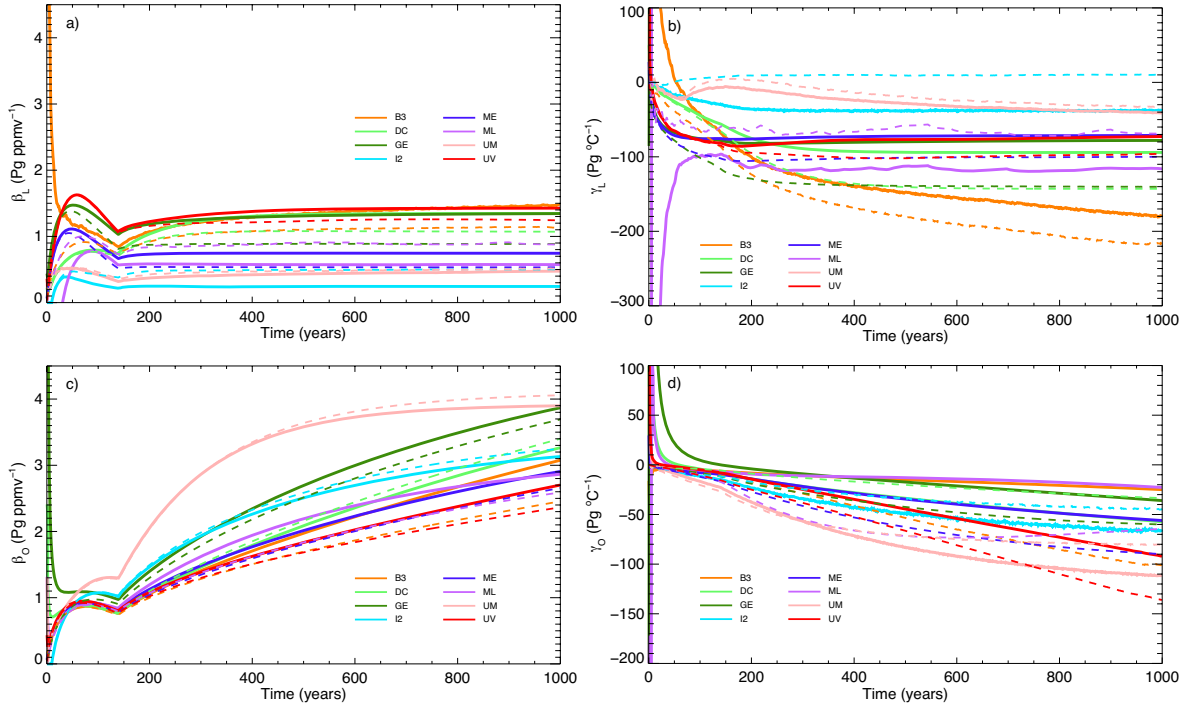

Fig. 6. Land and ocean carbon cycle sensitivities, diagnosed from a 1 % increase to $4 \times CO_2$ experiment, for models with land and ocean carbon cycle components. The CO_2 concentration–carbon sensitivity for land (β_L) is shown in **(a)** and for ocean (β_O) in **(c)**. The climate–carbon sensitivity for land (γ_L) is shown in **(b)** and for ocean (γ_O) in **(d)**. The solid lines indicate sensitivities calculated directly from partially coupled experiments while the dashed lines indicate sensitivities calculated indirectly as differences between partially and fully coupled experiments. See the main text for details.

large continuing change in γ_L in the B3 model is likely due to the inclusion of permafrost in that model, which reacts to climate change over much longer timescales than most other land processes. The I2 model has the lowest value of β_L, and this is likely due to nitrogen limitation reducing land uptake in this model (Sokolov et al., 2008). Over the ocean, the changes in both sensitivities, β_O and γ_O, largely occur after year 140 (CO_2 quadrupling). As expected, the response time of most land processes (possibly excluding permafrost and peat) is much faster than the response time of the ocean to either CO_2 or climate change.

The dashed lines in Fig. 6 show sensitivities calculated indirectly (as differences from fully coupled simulations). If γ_L is calculated indirectly, the I2 model indicates a positive rather than a negative land sensitivity (see Fig. 6b). This is due to a strong interaction between climate warming, which causes an increase in nitrogen availability and photosynthesis, and land carbon uptake. When calculated indirectly, the interaction is strong enough to change the climate–carbon feedback on atmospheric CO_2 from positive to negative for the I2 model. UM also has a positive γ_L for a short period when calculated indirectly, while all other models always show negative γ_L, using either method of calculation. UV, B3, GE and ME always show more negative γ and β, while I2 and UM always show more positive γ and β, when these sensitivities are calculated indirectly rather than directly. ML shows more positive sensitivities for land and more negative for the ocean, while DC is the opposite, when γ and β are calculated indirectly rather than directly. Presumably the nonlinear interactions that cause both γ and β to always change in the same direction (depending on the calculation method, for either the ocean or land) must be very different in the models.

Figure 7a shows the residence time of CO_2 emissions from a $4 \times CO_2$ pulse simulation. This pulse is equivalent to about 1800 Pg. As seen in Table 4, the EMIC mean time for half of the emitted CO_2 to be absorbed by the land and ocean sinks is 130 yr. This is considerably longer than the estimate of 30 yr to remove 50 % of emissions given in Chapter 7 of the AR4 (Denman et al., 2007). The main reason for this difference is that the emission pulses used to assess the CO_2 absorption timescales in the AR4 were small (40 Pg) compared to both the pulse used here and any likely future emissions. Absorption timescales depend on the amount of emissions (Maier-Reimer and Hasselmann, 1987; Archer et al., 2009; Joos et al., 2012), and this could have been stated more clearly in Chapter 7 of the AR4. Two models (B3 and ME) show considerably longer times to absorb half of emissions. The longer time for the B3 model is likely due to the increasing climate feedback over land due to the inclusion of permafrost and peat in that model.

The carbon-climate response has been proposed as a simple metric that combines both the climate and carbon cycle sensitivities into a single value. It has been suggested that this metric is relatively insensitive to emission scenarios and is approximately constant over several hundred years (Matthews et al., 2009). Figure 7b shows the CCR from a 1 % increasing CO_2 experiment which has zero emissions after reaching $4 \times CO_2$. The EMIC results show that, at least for this scenario, CCR is not constant over time for any of the models, although the intra-model range is smaller for most models than the inter-model range. This metric decreases in all models until emissions are set to zero. After CO_2 is allowed to freely evolve, CCR generally increases and then declines in most models. After emissions are set to zero, any changes in CCR are just due to changes in SAT and so

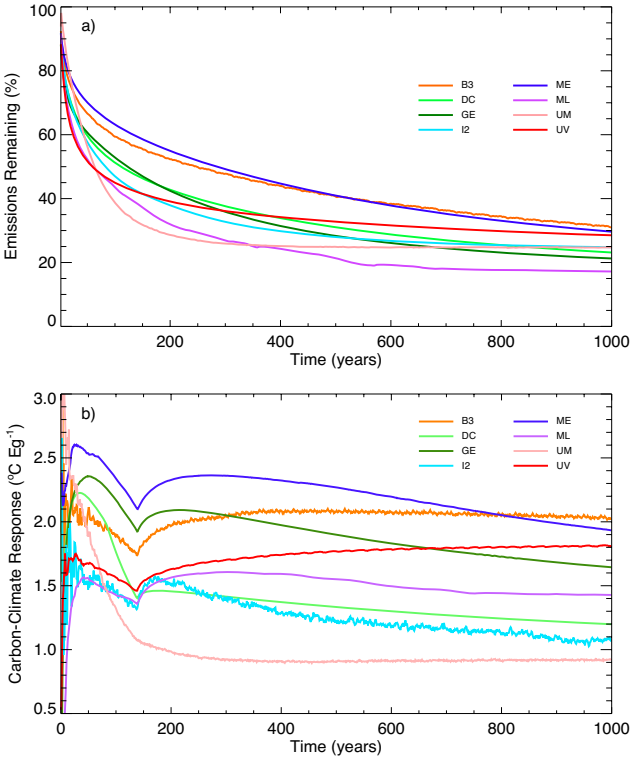

Fig. 7. Indicators of climate change longevity. The percentage of emissions remaining from a $4 \times CO_2$ pulse experiment is shown in **(a)**, and the carbon-climate response (CCR) from a 1 % increase to $4 \times CO_2$ experiment is shown in **(b)**. CO_2 is allowed to freely evolve in both experiments once CO_2 has reached 4 times the initial preindustrial level. This is equivalent to about 1800 Pg of carbon emissions. CCR is calculated as the change in SAT divided by the accumulated, diagnosed emissions. After year 140, emissions are zero and any changes in CCR are just due to changes in temperature.

CCR becomes a measure of a model's zero emissions commitment. Two models show a continual increase while one shows a continual decrease. At the time of CO_2 doubling, the range in CCR is between 1.4 and 2.5 °C Eg^{-1} of carbon (1 Eg or Tt = 1000 Pg or Gt), and after 500 yr the range is between 0.9 and 2.3 °C Eg^{-1}. Further discussion of the response of CCR in these models can be found in Zickfeld et al. (2013).

3.5 Contributions of forcing components to temperature

Several experiments were designed to examine the linearity of temperature and carbon cycle response to various climate forcings. In each experiment, only one major climate forcing was allowed to vary over the historical period (years 850 to 2005). The individual experiments applied forcing from "additional" or non-CO_2 greenhouse gases (AGG), CO_2 (CO2), land-use change (LUC), orbital (ORB), solar luminosity (SOL), sulphate aerosols (SUL) and volcanic aerosols (VOL). Figure 8 shows the EMIC mean results from

the individual forcing experiments compared to the experiment that applied all forcings together. Since specified CO_2 forcing is treated separately, any changes in CO_2 due to other forcings, either directly, as with land-use change, or indirectly, through climate–carbon feedbacks, are included as part of the CO_2 forcing.

As expected, most of the change in SAT over the last millennium has occurred after industrialization (Fig. 8a). Since 1800, the direct albedo effect from land-use change caused a model average cooling of roughly 0.2 °C, while sulphate forcing also caused a cooling of about 0.2 °C. The sulphate forcing may seem weak, but it is mostly due to the exclusion of the indirect forcing from sulphates in the experimental design. The lack of negative forcing from the indirect effect of sulphates is balanced by also excluding similar positive forcing from ozone and black carbon (see Appendix B). The change in solar luminosity since 1800 was found to have a small positive effect on SAT (< 0.1 °C). Non-CO_2 greenhouse gases have had a large influence on SAT since 1800, but this is largely countered by the combined negative forcing from land use and aerosols. As a result, CO_2 alone is capable of providing the vast majority of the climate change signal since pre-industrial times.

Before industrialization, the net changes in SAT from any of the forcings over the previous 1000 yr are much weaker, although there are warmer and cooler periods during that time (Fig. 8b). It appears that changes in solar forcing have the largest effect on SAT over long timescales in these simulations. Over the last millennium, orbital forcing was found to have almost no effect on modelled SAT, at the hemispheric scale, in the annual mean, while LUC is associated with a small long-term cooling. Volcanic aerosol forcing has a large but short-lived negative effect on modelled SAT. This agrees with the conclusions of Shindell et al. (2003) and Fernández-Donado et al. (2012), although Schneider et al. (2009), Feulner (2011), Miller et al. (2012), and Schleussner and Feulner (2012) indicate the possibility of large volcanic forcing causing longer term persistent cooling in polar regions. Volcanic forcing does, however, contribute to the cooling between the MCA and the LIA because of the larger number of big eruptions during the latter period (see also Fig. 11).

As noted earlier, the models appear to underestimate the SAT changes between the MCA and the LIA compared to reconstructions (Mann et al., 2008; Frank et al., 2010). With similar forcing, the CMIP5 models also show a similar small change in SAT simulated over this period (Fig. 1c). A relatively small change in simulated SAT between the MCA and LIA is also seen in Fig. 15 of Goosse et al. (2010). The low solar variation simulations (E1) of Jungclaus et al. (2010) similarly show small longer term (> 100 yr) changes in SAT between the MCA and LIA (see their Fig. 3), although shorter term variability can produce larger differences. Fernández-Donado et al. (2012) show that models (EC5MP-E1 and CSIRO; see their Fig. 1) with low, long-term solar variability (labelled ssTSI and similar to the

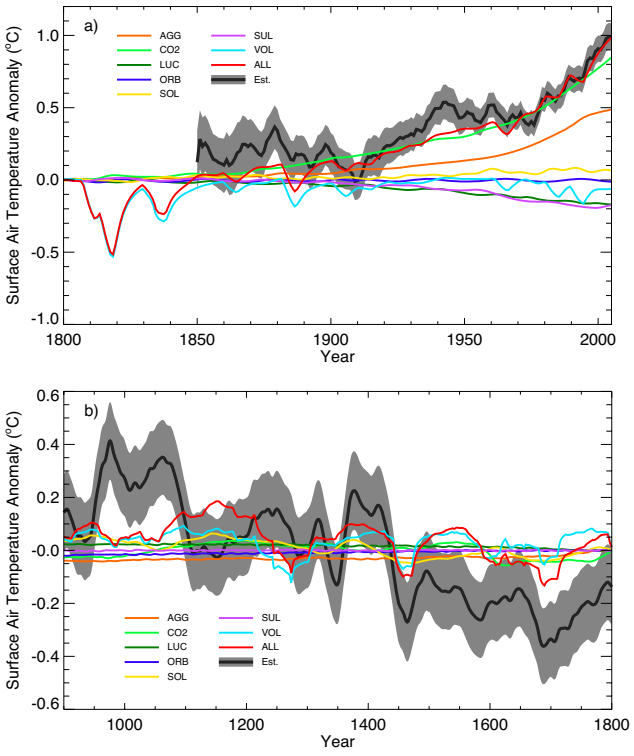

Fig. 8. Individual forcing component contributions to the total global surface air temperature response. The model results are from the average of 11 models: B3, C2, C3, DC, GE, I2, LO, MI, ME, UM and UV. The response after 1800 is shown in **(a)**. The dark grey line shows changes in global SAT, and the grey shading indicates the uncertainty, from Morice et al. (2012). The model results and the data estimates were processed with a 5 yr moving average, rectangular filter. Model results are shown as anomalies from the decade centred at 1800. The data estimates are shown as an anomaly, which has been offset to show the same SAT anomaly as the all-forcing average over the decade centred on the year 1900. The response before 1800 is shown in **(b)**. The dark grey line shows changes in global SAT, and the grey shading indicates the uncertainty, from the EIV reconstruction of Mann et al. (2008). Model results and data estimates are shown as anomalies from their average over the entire period (850 to 1850) and have been processed with a 30 yr moving average, rectangular filter.

Schmidt et al. (2012) solar forcing used here) simulate very small SAT changes between the MCA and LIA (~ 0.1 °C; see their Fig. 6).

With similar solar forcing to the datasets used here, many models are not capable of generating a large enough MCA to LIA temperature transition when compared to reconstructions (but see Feulner, 2011). Additionally, several studies have argued that internal variability may have played a significant role in explaining temperature changes during the past millennium (e.g. Jungclaus et al., 2010; Goosse et al., 2012). The models and experimental design used here do not take into account this potential contribution, and this may explain part of the disagreement between model results and reconstructions.

3.6 Linearity of the forced response

Figure 9a shows the difference between the anomalous response of the all-forcing experiment and the sum of the anomalous responses of the individual forcing simulations. If the climate system responded linearly to the individual forcings, then the resulting summation would be zero. In general this is the case for all models. There are some differences after 1900 for the ME and UM model, but these differences are still small compared to overall noise. It may be that EMICs are too simple to demonstrate significant nonlinearities, but given the diversity in the complexity of EMICs, this seems unlikely. Fernández-Donado et al. (2012) also suggest a high degree of linearity between forcing and simulated temperature.

Figure 9b shows similar results for diagnosed carbon emissions. Here some models appear to show an interaction between individual forcing that is larger than noise, particularly the UV model. This interaction is between land-use change and CO_2 forcing. In models that simulate land-use forcing by removing vegetation (B3, GE, I2 and UV), it would be expected that there would be less CO_2 fertilization due to the removal of vegetation from land-use change (Strassmann et al., 2008). This reduction in land uptake by CO_2 fertilization would result in lower diagnosed emissions and thus total carbon in a simulation that has both land-use change and CO_2 fertilization acting together. In the DC model most of the land carbon removed by land-use change was taken from the soil rather than from the vegetation and so this model would not be expected to show a strong interaction. The ME and UM models also do not show this interaction between vegetation removal (due to land-use change) and the CO_2 fertilization feedback since they do not reduce vegetation or directly exchange carbon with land use. The UV model has one of the largest CO_2 concentration–carbon sensitivities (Table 4) and the largest recent land-use emissions (Table 3). As such, it shows the largest interaction between land-use change and CO_2. The GE model is not shown, because one of the ensemble members that constitute the ensemble mean was not useable.

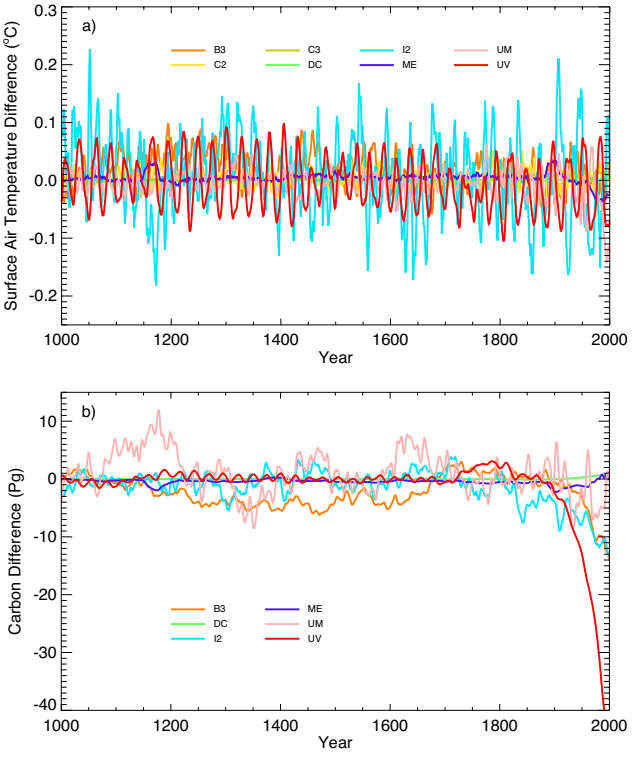

Fig. 9. The linearity of the surface air temperature response **(a)** and carbon fluxes to the atmosphere **(b)** over the last millennium. Differences are between anomalies from the all-forcing simulation and the sum of the anomalies from all of the individual forcing component simulations. Model results have been processed with a 5 yr moving average, rectangular filter. The differences are shown as anomalies from the average of the century centred at about year 1000. If the individual component responses added linearly to the total response, then the differences should be zero.

3.7 Changes in climate from natural and anthropogenic forcing

Freely evolving CO_2 simulations have the advantage of not forcing the model into a specified state. Thus, these types of experiments can show how CO_2 might change under different scenarios. Two historical simulations in which CO_2 was allowed to freely evolve were conducted to determine the anthropogenic influence on the carbon cycle. While one simulation applied natural forcing, the other included natural and anthropogenic forcing, including specified emissions from fossil fuel combustion. The anomalous SAT from these two simulations since 1750 is shown in Fig. 10. The range in the simulations with only natural forcing is very small compared to the range of the models when anthropogenic forcing is also applied. This is not surprising since the magnitude of the anthropogenic forcing is much greater than the magnitude of the natural forcing, so any differences in model response are amplified. The simulations with only natural forcing produce almost no change in overall SAT between 1750 and 2005. As seen in many other studies (see Hegerl et al., 2007 for a review), when only natural forcing is applied, the models are not capable of simulating the rise in SAT that has been observed over this time period.

It is important to understand the feedbacks between the carbon cycle and the climate system in order to have confidence in future projections. Most models show a positive climate–carbon cycle feedback (Friedlingstein et al., 2006). However, the magnitude, the constancy and perhaps even the sign of the feedback are still uncertain (Sokolov et al., 2008). Reconstructions of past climate variables and forcing, combined with carbon cycle model simulations, may help constrain model climate–carbon cycle feedbacks. On the other hand, climate reconstructions are also often highly uncertain

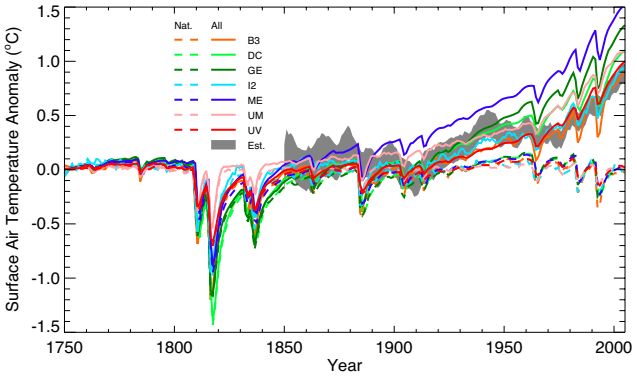

Fig. 10. The surface air temperature response of the models in freely evolving CO_2 simulations that include only natural forcing (Nat.) or all-forcing (All). Note all-forcing includes both natural (orbital, solar, stratospheric and volcanic aerosols) and anthropogenic (greenhouse gas, land use, tropospheric aerosol) forcing. As in Fig. 7, the light grey shading indicates the uncertainty range in SAT, from Morice et al. (2012). The model results and the data estimates were processed with a 5 yr moving average, rectangular filter. Model results are shown as anomalies from the decade centred at 1750. The data uncertainty estimates are shown as an anomaly, which has been offset to show the same SAT anomaly as the model average over the decade centred on the year 1900.

and disparate. Models may then be useful in assessing the plausibility of differing palaeoclimate reconstructions, by allowing reconstructions and forcing to be compared in a physically consistent manner.

3.8 Changes in temperature between the MCA and the LIA

The pre-industrial SAT anomalies from the naturally forced, freely evolving CO_2 simulation are shown in Fig. 11a. The models simulate a modest MCA and a small decline in SAT into the LIA that is similar to the specified CO_2 experiment. Although there is considerable uncertainty, estimates from palaeoclimate reconstructions suggest about 0.38 °C as the difference between the warmest (1071–1100) and coolest (1601–1630) pre-industrial periods in the Northern Hemisphere over the last millennium (Frank et al., 2010). The start and end of these climate periods are still debated, but for the simple analysis used here we define an MCA index period to be between 1100 and 1200, and a LIA index period between 1600 and 1700. The 100 yr periods used for these indices were chosen to represent the models' warmest period between year 950 and 1250 and the coolest period between 1450 and 1750. These periods are slightly later than the times estimated from reconstructions for the highest and lowest temperature change for the pre-industrial portion of the last millennium (Frank et al., 2010). Between these 100 yr MCA and LIA periods, the model average difference in globally averaged SAT is 0.19 °C. The largest difference occurs in GE, which simulates a drop in temperature of 0.33 °C between the reference periods.

For the all-forcing simulation (with land-use change and specified CO_2), the average EMIC global SAT response for the transition between the MCA and the LIA index periods is about 0.21 °C (see Fig. 11b). The slightly smaller change in SAT in the naturally forced, free CO_2 simulation is in part due to the lack of cooling from land-use change (which is not included in the natural forcing simulation), but mostly because the simulated drop in CO_2 is not as great as suggested from ice cores (see Fig. 11c). With the additional cooling from the specified reduction in CO_2, the largest difference once more occurs in GE, which simulates a drop in temperature of 0.35 °C. It is, however, difficult to compare SAT changes averaged over different periods and regions. For example, the UV model simulates a 0.05 °C greater drop in SAT over the Northern Hemisphere (for which the observational estimate was reconstructed) than globally. However, even after correcting for this difference, most models appear to be underestimating the change in SAT over this period.

The lack of cooling in the models may be from underestimating the specified forcing changes over this period. The individual forcing component contributions to the change in SAT are shown in Fig. 11b. The CO_2, solar and volcanic forcings are, in nearly equal proportions, the major contributors to the total drop in SAT between the MCA and the LIA index periods. There is also a small cooling contribution from the direct climate effects of land-use change, and very small warming contributions from changes in orbit and non-CO_2 greenhouse gases. There are earlier periods in the simulations that are as cold or nearly as cold as the LIA index period. These early minima in simulated temperature are mostly caused by a series of volcanic eruptions.

3.9 Changes in CO_2 between MCA and LIA

CO_2 can be extracted directly from ice cores and is relatively well reconstructed over the past millennium, although there are still uncertainties in both the timing of the CO_2 record and in determining how well CO_2 records from individual ice cores represent global values. The large fluctuations in modelled CO_2 before the LIA are not seen in the PMIP3 CO_2 dataset (Fig. 11c and d), although other records may be more variable (Mitchell et al., 2011). If we assume that the CO_2 record is accurate and that changes in CO_2 are determined by changes in SAT over this period (through climate–carbon cycle feedbacks), then there would appear to be an inconsistency between the lack of change in the CO_2 record and the large model temperature changes generated by the (mostly volcanic) forcing before the LIA. This implies the following: the specified volcanic forcing is not realistic, or the CO_2 record is not reliable, or the climate–carbon cycle feedback is weak or masked in the CO_2 record by other factors. It is beyond the present experiment to say which is the case, but this does warrant more research.

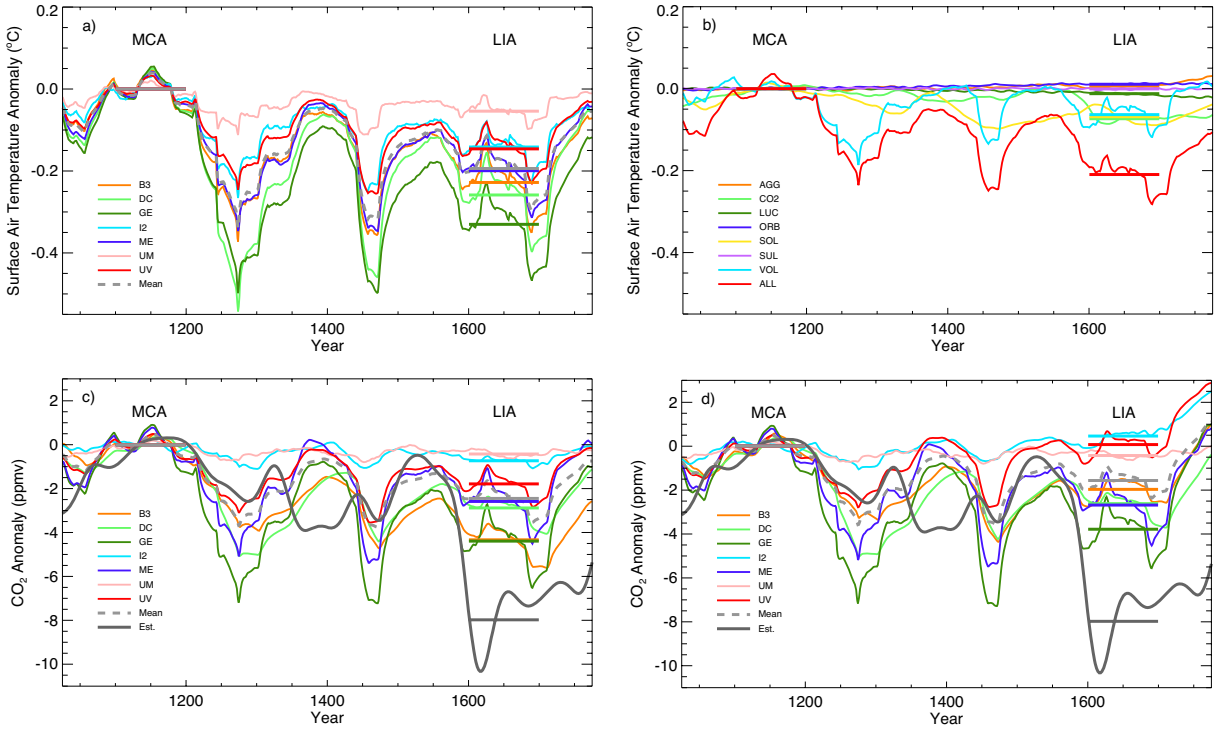

Fig. 11. Comparison of global surface temperature and CO_2 responses over the preindustrial portion of the last millennium. The surface air temperature responses in **(a)** are from the freely evolving CO_2 simulations with only natural forcing. The contributions of individual forcing components to the temperature response, shown in **(b)**, are model averages from experiments with specified CO_2. The model averages in **(b)** are from 11 models: B3, C2, C3, DC, GE, I2, LO, MI, ME, UM and UV. Maximum Northern Hemisphere SAT changes between the MCA and LIA are estimated to be about 0.4 °C from palaeoclimate reconstructions, but this is highly uncertain (Frank et al., 2010). The CO_2 response is shown for the freely evolving CO_2 simulations with only natural forcing in **(c)** and all-forcing in **(d)**. When multiple model results are shown, the model mean is indicated by a dashed grey line. The solid dark grey lines in **(c)** and **(d)** are an estimate of reconstructed CO_2 from the PMIP3 forcing dataset (Schmidt et al., 2012). Horizontal lines over two, century-long index periods (1100–1200 and 1600–1700), which roughly correspond to the Medieval Climate Anomaly (MCA) and Little Ice Age (LIA), indicate model or data averages over these periods. All model results and data estimates are shown as anomalies from the average over the years 1100 to 1200 and were processed with a 30 yr moving average, rectangular filter.

Along with temperature, the models also seem to underestimate the reduction in CO_2 during the MCA–LIA transition. The model average reduction in CO_2 is 2.4 ppm compared to 7.9 ppm from the PMIP3 protocol reconstruction (Schmidt et al., 2012), calculated over the same MCA and LIA index periods. Since most models appear to have a positive climate–carbon cycle feedback over this period (see Fig. 11a and c), some of the small reduction in CO_2 would be attributable to an underestimated reduction in SAT.

3.10 Estimating the carbon-climate sensitivity from the MCA to LIA transition

Assuming all of the reduction in CO_2 is driven by changes in climate, a crude estimate of the climate feedback can be calculated from the simulated change in CO_2 and SAT over the MCA–LIA transition. This estimate of the climate–carbon cycle sensitivity has a model average of 2.4 ppm/0.19 °C = 12.6 ppm °C^{-1}, with a range between 5.1 and 18.8 ppm °C^{-1}. This estimate is relatively insensitive to the reference periods. Using the average change in SAT and CO_2 between 950 to 1250, and 1450 to 1750 yields very similar results (model average of 13.5 ppm °C^{-1} with a range between 4.5 and 23.3 ppm °C^{-1}). If this estimate of sensitivity were to hold for larger changes in temperature, then the model average drop in CO_2 for a 0.4 °C reduction in temperature would be 5.1 ppm. Even scaling the response of the model with the largest sensitivity (18.8 ppm °C^{-1} for B3) would still only produce a drop in CO_2 of 7.5 ppm. Apparently, in order to simulate the large observed drop in CO_2 during the MCA–LIA transition, either the temperature drop must be larger than 0.4 °C or the climate–carbon cycle feedback must be large ($>$ 18 ppm °C^{-1}).

Few models have attempted to simulate a closed carbon cycle over the past millennium. Gerber et al. (2003) used a carbon cycle model with a sensitivity of about 12 ppm °C^{-1} to constrain the temperature transitions over the pre-industrial portion of the last millennium to less than

1 °C. Both Goosse et al. (2010) and Jungclaus et al. (2010) have used sophisticated models to simulate the evolution of CO_2 over the past millennium. Goosse et al. (2010) show almost no change in CO_2 between the MCA and LIA (see their Fig. 16), and Jungclaus et al. (2010) also seem to underestimate the reduction in CO_2 over this period (see their Fig. 6). As with the models in this study, some of the small reduction in CO_2 in Goosse et al. (2010) and Jungclaus et al. (2010) is likely due to the small reduction in simulated SAT between the MCA and LIA. It seems that many models are not able to reproduce the reduction in CO_2 shown in the PMIP3 protocol reconstruction (Schmidt et al., 2012) over this period.

The direct comparison of EMIC model results with proxy data reconstructions over the last millennium is hampered by the large uncertainty in developing annual-mean proxies from sporadic point source measurements in space and time. Inherent internal variability in the climate system may also make it difficult to compare EMICs, which show little internal variability, to the palaeorecord, which is a single sample of the climate system's natural variability. In addition, our EMIC results are globally averaged and there are few proxy records in the Southern Hemisphere so that current SAT reconstructions focus only on the Northern Hemisphere records. Even after accounting for the different areas and averaging periods over which the MCA and LIA are defined, results suggest that the models may be underestimating both the drop in SAT and CO_2 during the transition from the MCA into the LIA. This in turn could be the result of inadequately modelled, large, long-term, unforced climate variability, errors in the reconstructions of volcanic and/or solar radiative forcing used to drive the models, or the incomplete representation of certain processes within the models.

It is possible that past changes in CO_2 are unrelated to changes in SAT. Long timescale natural variability, unrelated to any climate–carbon feedbacks, could be responsible for many of the past large changes in SAT or CO_2. If preindustrial land-use changes were significant, then land-use emissions to the atmosphere would also alter the climate–carbon sensitivity estimated from palaeoclimate records. While the effects of unresolved variability are difficult to assess, the possible influence of land-use change on the diagnosed palaeoclimate–carbon sensitivity can be investigated with the freely evolving CO_2 experiments. The evolution of CO_2 in the simulation including anthropogenic forcing, which before 1800 was almost entirely from land-use change, is shown in Fig. 11d. Including anthropogenic forcing reduces the model average estimate of the climate–carbon cycle sensitivity from 12.6 to 8.4 ppm $°C^{-1}$. Other land-use reconstructions, which suggest larger pre-industrial land-use fluxes (as in Kaplan et al. 2010), may result in an even larger reduction in apparent sensitivity. However, if the models simulated a larger reduction in CO_2 between the MCA and LIA (due to a higher sensitivity), then, proportionally, the influence of modelled land-use emissions on estimates of the palaeoclimate–carbon cycle sensitivity would be smaller. This result clearly depends on the simulation of uncertain land-use change, but at least for these experiments, there is a considerable sensitivity in diagnosing climate–carbon feedbacks when including emissions from land-use change.

4 Conclusions

We have evaluated EMIC simulations over the last millennium with respect to other models and historical data. Although some model defects are noted, the EMICs in this intercomparison generally perform well. There is a large range in initial pre-industrial model state, at least in terms of SAT (12.3 to 17.3 °C), but this seems to have little relationship to the models' transient responses to recent changes in radiative forcing. A few models appear to overestimate ocean heat uptake and sea level rise compared to observational estimates over the last several decades. All models show a small decline in the Atlantic meridional overturning circulation over the last century. Ocean carbon uptake is well simulated by all models (within observational uncertainty estimates), but recent land carbon uptake appears to be slightly underestimated by most models. The low land uptake is likely not due to an overestimation of land-use change emissions, which are generally underestimated, but due to overly low residual uptake. This may be due to an overestimation of climate–carbon feedbacks, but is more likely due to an underestimation of the fertilization of photosynthesis.

Idealized experiments were used to calculate a number of standard climate and carbon cycle metrics. The range in the transient climate response is similar to that of CMIP3 and CMIP5 models (Andrews et al., 2012). The model climate sensitivities (diagnosed at year 1000 from 2 × pulse experiments) range from 1.9 to 4.0 °C, spanning most of the likely range given in the IPCC AR4 (2.0 to 4.5 °C). The model average climate sensitivity is 3.0 °C. The models also show a large range in the carbon cycle, CO_2 concentration and climate feedbacks, but all models show negative concentration feedbacks and most show positive climate feedbacks. The carbon climate response (CCR) is not constant for most models either before or after emissions cease, which suggests caution when using this metric. On average, the models suggest that the time to absorb half of an atmospheric CO_2 perturbation (from a relatively large pulse of approximately 1800 Pg) is 130 yr (also see Joos et al., 2012).

The linearity of the climate and carbon cycle components and the importance of different external forcings were assessed with a series of simulations in which each forcing was applied separately. In general, the SAT of a simulation with all forcings is well represented by the sum of the individual forcings. This is not always the case with diagnosed emissions, due to interactions between changing land-use and CO_2 concentrations, for some models. The response of the all-forcing simulations is very similar to simulations with only CO_2 forcing. This implies that historical

and modern-day climate forcing can largely be captured by CO_2, alone, as most other forcings tend to cancel.

Free CO_2 simulations were also performed to assess how CO_2 might evolve under different forcing scenarios. Simulations without anthropogenic forcing show almost identical SAT and CO_2 in 2005 compared to 1750. It is only when anthropogenic forcing is added that the models warm by 0.8 °C, on average, over the 20th century.

The climate–carbon sensitivity over the preindustrial portion of the last millennium was compared to palaeoclimate proxy estimates. The uncertainties in palaeoclimate estimates of model forcing and climate make it difficult to constrain the models' climate–carbon cycle response. None of the models were able to reproduce the reconstructed drop in SAT or CO_2 during the MCA to LIA transition.

The effects of land-use emissions on estimates of climate–carbon cycle sensitivities were assessed, and these were found to significantly reduce the diagnosed sensitivity. This suggests that land-use emissions need to be considered when making estimates of climate–carbon feedbacks from palaeoclimate reconstructions. While some of our conclusions remain tentative, our analyses suggest that EMICs can be useful tools in helping to reconcile different palaeoclimate proxy datasets in a physically consistent manner.

Appendix A

Model descriptions

– *B3*: Bern3D-LPJ is an Earth system model of intermediate complexity with a fully coupled carbon cycle and components that represent the ocean and sea ice, the ocean sediments, the atmosphere, and the terrestrial biosphere. The ocean component is a seasonally forced three-dimensional frictional geostrophic global ocean model with a resolution of 36×36 boxes in the horizontal direction and 32 vertical layers (Edwards et al., 1998; Müller et al., 2006). Marine biogeochemical cycles are implemented following OCMIP-2 (Najjar and Orr, 1999; Orr et al., 2000) with the addition of prognostic formulations for biological productivity and the cycling of iron, silica, ^{13}C and ^{14}C (Parekh et al., 2008; Tschumi et al., 2008), as well as a sedimentary component (Tschumi et al., 2011; Gehlen et al., 2006; Heinze et al., 1999). The atmosphere is represented by a single-layer energy and moisture balance model with the same horizontal resolution as the ocean component (Ritz et al., 2011). The CO_2 forcing is calculated after Myhre et al. (1998) and the model is tuned to produce an equilibrium climate sensitivity of 3 °C (global mean SAT increase for a doubling of preindustrial CO_2, excluding land albedo and other terrestrial feedbacks). Other greenhouse gases and volcanic aerosols are prescribed as global radiative forcing, while tropospheric sulphate aerosols are taken into account by changing the surface albedo locally (Steinacher, 2011; Reader and Boer, 1998). The terrestrial biosphere component is based on the Lund-Potsdam-Jena (LPJ) dynamic global vegetation model at $3.75° \times 2.5°$ resolution (Joos et al., 2001; Gerber et al., 2003; Sitch et al., 2003). Vegetation is represented by 12 plant functional types, and CO_2 fertilization is modelled according to the modified Farquhar scheme (Farquhar et al., 1980). The model has recently been extended with modules to account for land use (Strassmann et al., 2008; Stocker et al., 2011), peatlands and permafrost dynamics (Gerten et al., 2004; Wania et al., 2009a,b), and land surface albedo (Steinacher, 2011). The LPJ component is driven by global mean CO_2 concentrations and changes in surface air temperature relative to a reference period using a pattern scaling approach (Stocker et al., 2011; Steinacher, 2011).

– *C2*: The CLIMBER-2.4 model (Petoukhov et al., 2000; Ganopolski et al., 2001) is a fully coupled climate model without flux adjustments. It consists of a 2.5-dimensional statistical–dynamical atmosphere module with a coarse spatial resolution of 10° in latitude and 360°/7 in longitude, which does not resolve synoptic variability. The vertical structures of the temperature and humidity are parameterized as well. The ocean component has three zonally averaged basins with a latitudinal resolution of 2.5° and 20 unequal vertical levels. The model also includes a zonally averaged sea ice module, which predicts ice thickness and concentration and includes ice advection.

– *C3*: The intermediate complexity climate model CLIMBER-3α (Montoya et al., 2006) shares CLIMBER-2's statistical–dynamical atmosphere (Petoukhov et al., 2000), but operates at a higher horizontal resolution of 22.5° in longitude and 7.5° in latitude. Additionally, it employs a general circulation model for the ocean component. This ocean module is based on MOM3 (Pacanowski and Griffies, 1999), but includes a second-order moments tracer advection scheme (Hofmann and Morales Maqueda, 2006) as well as changes to the parameterizations of diffusivity and convection (Montoya et al., 2006). In CLIMBER-3α, the ocean model has a horizontal resolution of 3.75° in both latitude and longitude. It divides the ocean into 24 vertical levels of variable height, ranging from 25 m at the surface to about 500 m at the largest depths. Sea ice is represented by the thermodynamic–dynamic sea ice model ISIS (Fichefet and Morales Maqueda, 1997). Land surface types (including vegetation) are prescribed in the coupler.

– *DC*: The DCESS model consists of fully coupled modules for the atmosphere, ocean, ocean sediment, land biosphere and lithosphere (Shaffer et al., 2008). The

model geometry consists of one hemisphere, divided into two 360° × 52° zones. Long-term climate sensitivity has been calibrated to 3 °C. The atmosphere component considers radiation balance, heat and gas exchanges with other modules, and meridional transport of heat and water vapour between low–midlatitude and high latitude zones. The ocean component is 270° wide and extends from the Equator to 70° latitude. Both ocean sectors are divided into 55 layers with 100 m vertical resolution. Each layer is assigned an ocean sediment section, with width determined from observed ocean depth distributions. Sea ice and snow cover are diagnosed from estimated atmospheric temperature profiles. Circulation and mixing are prescribed, with values calibrated from observations as in the HILDA model (Shaffer and Sarmiento, 1995). The ocean sediment component considers calcium carbonate dissolution as well as oxic/anoxic organic matter remineralization. The land biosphere component includes leaves, wood, litter and soil. For this experiment, it has been modified to include prescribed land-use change carbon losses, distributed in proportion to the initial inventory sizes of the module components. With this change, the model CO_2 fertilization factor, originally 0.65, has been recalibrated to 0.37. Finally, the lithosphere component considers outgassing and climate-dependent weathering of carbonate and silicate rocks, as well as rocks containing old organic carbon and phosphorus.

– *FA*: FAMOUS (Smith et al., 2008) is a low resolution AOGCM with no flux adjustments, based on the widely used HadCM3 climate model (Gordon et al., 2000). The atmosphere component is the primitive equation model HadAM3 (Pope et al., 2000), with resolution 5° × 7.5° and 11 vertical levels. It uses an Eulerian advection scheme, with a gravity-wave drag parameterization. Radiative transfer is modelled using six shortwave bands and eight longwave bands, while convection follows a mass-flux scheme, with parameterizations of convective downdrafts and momentum transport. Some of the parameter values in HadAM3 which are poorly constrained by observations have been systematically tuned so that FAMOUS produces a climate more like that of HadCM3 (Jones et al., 2005; Smith et al., 2008). FAMOUS uses a coastal tiling scheme which combines the properties of land and sea in coastal grid boxes in the atmosphere model. The ocean component is HadOM3 (Gordon et al., 2000; Cox, 1984). The resolution is 2.5° × 3.75°, with 20 vertical levels. It is a rigid lid model, where surface freshwater fluxes are converted to virtual tracer fluxes via local surface tracer values. HadOM3 uses isopycnal mixing and thickness diffusion schemes with a separate surface mixed layer, while diapycnal mixing of momentum below the mixed layer is parameterized using a Richardson-number dependent scheme. The momentum equations are slowed by a factor of 12 with Fourier filtering applied at high latitudes to smooth instabilities. Outflow from the Mediterranean is parameterized by simple mixing between an area in the Atlantic and an area in the Mediterranean from the surface to a depth of 1300 m. Iceland has been removed to facilitate ocean heat transport, and an artificial island is used at the North Pole to alleviate the problem of converging meridians. The sea-ice component uses simple, zero-layer thermodynamics, which is advected with the surface ocean currents. Land processes are modelled via the MOSES1 land surface scheme (Cox et al., 1999).

– *GE*: The GENIE-1 physical model comprises the 3-D frictional geostrophic ocean model GOLDSTEIN, at 10° × (3–19)° horizontal resolution with 16 vertical levels, coupled to a 2-D energy moisture balance atmosphere and a thermodynamic–dynamic sea-ice model (Edwards and Marsh, 2005). Recent developments (Marsh et al., 2011) include the incorporation of stratification-dependent mixing, a more general equation of state through a parameterization of thermo-baricity, and improvements to the representation of fixed wind forcing. The land surface component is ENTS, a dynamic model of terrestrial carbon storage (Williamson et al., 2006) with a relatively simple implementation of spatiotemporal land-use change (Holden et al., 2013). Ocean chemistry is modelled with BIOGEM (Ridgwell et al., 2007), including iron limitation (Annan and Hargreaves, 2010), and is coupled to the sediment model SEDGEM with fixed weathering, diagnosed during the model spin-up to simulated observed ocean alkalinity (Ridgwell and Hargreaves, 2007). All GENIE results are derived from ensembles applying the same 20-member parameter set. The selected parameters were filtered from a 100-member, 28-parameter pre-calibrated ensemble, constrained for plausible present-day CO_2 concentrations.

– *I2*: The MIT-IGSM2.2 (Sokolov et al., 2005) is an Earth system model of intermediate complexity. The atmospheric component is a zonally averaged primitive equation model (Sokolov and Stone, 1998) with 4° latitudinal resolution and 11 vertical levels. Each zonal band can consist of land, land ice, ocean, and sea ice. Surface temperature, turbulent and radiative fluxes, and their derivatives are calculated over each type of surface. The ocean component is a mixed layer/seasonal thermocline model with 4° × 5° horizontal resolution. Heat mixing into the deep ocean is parameterized through diffusion of the temperature anomaly at the bottom of the seasonal thermocline (Hansen et al., 1984). Embedded in the ocean model are a thermodynamic sea ice model and a carbon cycle model (Holian et al., 2001). The terrestrial model is comprised of CLM3.5 (Oleson et

al., 2008) for surface heat fluxes and hydrological processes, TEM (Melillo et al., 1993; Felzer et al., 2004) for carbon dynamics of terrestrial ecosystem, and NEM (Liu, 1996) for methane and nitrogen exchange. The coupled CLM/TEM/NEM model system represents the geographical distribution of land cover and plant diversity through a mosaic approach, in which all major land cover categories and plant functional types are considered over each cell, and are area-weighted to obtain aggregate fluxes and storages. A distinguishing feature of TEM is explicit interactions between the terrestrial carbon and nitrogen cycles (Sokolov et al., 2008). These simulated carbon/nitrogen interactions allow the model to consider the limiting effects of nitrogen availability on plant productivity and how changes in this availability from changing environmental conditions, such as warming (Sokolov et al., 2008) or the application of nitrogen fertilizers (Felzer et al., 2004), might influence future uptake and storage of carbon. For this study, the model also assumes that no nitrogen fertilizers were applied to croplands before 1950, but then after 1950, the proportion of fertilized croplands increased linearly until all croplands were assumed to be fertilized by 1990 and afterwards.

– *IA*: The IAP RAS climate model (Muryshev et al., 2009; Eliseev and Mokhov, 2011) employs a multilayer statistical–dynamical atmosphere component with a comprehensive radiation scheme, interactive cloudiness, and parameterized synoptic-scale fluxes. The ocean component is a primitive equation global circulation model developed at the Institute of Numerical Mathematics, Russian Academy of Sciences. The sea ice component uses a zero-layer thermodynamic scheme with two-level ice thickness distribution (level ice and leads). IAP RAS includes a comprehensive soil scheme with a high vertical resolution (Arzhanov et al., 2008), as well as a terrestrial and oceanic carbon cycle (Eliseev and Mokhov, 2011). Ice sheets are prescribed. The model does not use flux adjustments for coupling between the model components.

– *LO*: LOVECLIM 1.2 (Goosse et al., 2010) consists of components representing the atmosphere (ECBilt), the ocean and sea ice (CLIO), the terrestrial biosphere (VECODE), the oceanic carbon cycle (LOCH) and the Greenland and Antarctic ice sheets (AGISM). ECBilt is a quasi-geostrophic atmospheric model with 3 levels and a T21 horizontal resolution (Opsteegh et al., 1998). It includes simple parameterizations of the diabatic heating processes and an explicit representation of the hydrological cycle. Cloud cover is prescribed according to present-day climatology. CLIO is a primitive equation, free-surface ocean general circulation model coupled to a thermodynamic–dynamic sea ice model (Goosse and Fichefet, 1999). Its horizontal resolution is $3^\circ \times 3^\circ$ with 20 levels in the ocean. VECODE is a reduced-form model of vegetation dynamics and of the terrestrial carbon cycle (Brovkin et al., 2002). It simulates the dynamics of two plant functional types (trees and grassland) at the same resolution as that of ECBilt. A potential fertilization of net primary production (NPP) by elevated atmospheric CO_2 is accounted for by a logarithmic dependence of NPP on CO_2. LOCH is a comprehensive model of the oceanic carbon cycle (Mouchet and François, 1996). It takes into account both the solubility and biological pumps, and runs on the same grid as CLIO. Finally, AGISM is composed of a three-dimensional thermomechanical model of ice sheet flow, a viscoelastic bedrock model and a model of mass balance at the ice–atmosphere and ice–ocean interfaces (Huybrechts, 2002). For both ice sheets, calculations are made on a 10 km by 10 km resolution grid with 31 sigma levels. Note that LOCH and AGISM were not activated in the experiments conducted for this intercomparison.

– *ME:* MESMO version 1 (Matsumoto et al., 2008) is based on the C-GOLDSTEIN ocean model (Edwards and Marsh, 2005). It consists of a frictional geostrophic 3-D ocean circulation model coupled to a dynamic–thermodynamic sea ice model and atmospheric model of energy and moisture balance. Ocean production is based on prognostic nutrient uptake kinetics of phosphate and nitrate with dependence on light, mixed layer depth, temperature, and biomass. Interior ocean ventilation is well calibrated against natural radiocarbon on centennial timescale and against transient anthropogenic tracers on decadal timescale. Here MESMO1 is coupled to a simple prognostic land biosphere model (Williamson et al., 2006) that calculates energy, moisture, and carbon exchanges between the land and the atmosphere. Prognostic variables include vegetation and soil carbon as well as land surface albedo and temperature.

– *MI*: MIROC-lite (Oka et al., 2011) consists of a vertically integrated energy moisture balance atmospheric model, an ocean general circulation model, a dynamic–thermodynamic sea ice model, and a single-layer bucket land-surface model. All model components have $4^\circ \times 4^\circ$ horizontal resolution, and the ocean has 35 vertical layers. In the atmosphere component, heat is transported via diffusion and moisture is transported via both advection and diffusion. Internal diagnosis of wind is switched off, and externally specified wind based on observations is used for the computation of moisture advection in the atmosphere and air–sea flux exchanges. To close the water budget, excess land water overflowing from the bucket model is redistributed homogeneously over the entire ocean grid. No explicit flux corrections for heat and water exchanges are applied.

– *ML*: MIROC-lite-LCM (Tachiiri et al., 2010) has the same physical components as MIROC-lite, except that equilibrium sensitivity is tuned for 3 °C, runoff water is returned to the nearest ocean grid, freshwater flux adjustment is used between the Pacific and the Atlantic, and internally diagnosed wind is used in the physical components. Additionally, the marine carbon cycle is represented with an NPZD model (Palmer and Totterdell, 2001) in which a fixed wind speed is used. Daily variability from a previous simulation of MIROC3.2 (Hasumi and Emori, 2004) is used to drive the annual cycle of the terrestrial vegetation model Sim-CYCLE (Ito and Oikawa, 2002). The vegetation model is coupled back to MIROC-lite-LCM on an annual basis. To decrease computational cost, the model has a coarser horizontal resolution of $6° \times 6°$ with 15 vertical layers in the ocean.

– *SP*: SPEEDO (Severijns and Hazeleger, 2009) is an intermediate complexity coupled climate model. The atmospheric component of SPEEDO is a modified version of the AGCM Speedy (Molteni, 2003; Kucharski and Molteni, 2003), having a horizontal spectral resolution of T30 with a horizontal Gaussian latitude-longitude grid (approximately 3° resolution) and 8 vertical density levels. Simple parameterizations are included for large-scale condensation, convection, radiation, clouds and vertical diffusion. The ocean component of SPEEDO is the CLIO model (Goosse and Fichefet, 1999). It has approximately a $3° \times 3°$ horizontal resolution, with 20 vertical layers ranging from 10 to 750 m in depth. It includes the sea ice model LIM (Fichefet and Morales Maqueda, 1997). A convective adjustment scheme, increasing vertical diffusivity when the water column is unstably stratified, is implemented. SPEEDO also includes a simple land model, with three soil layers and up to two snow layers. The hydrological cycle is represented with the collection of precipitation in the main river basins and outflow in the ocean at specific positions. Freezing and melting of soil moisture is included.

– *UM*: The UMD Coupled Atmosphere–Biosphere–Ocean model (Zeng et al., 2004) is an Earth system model with simplified physical climate components including a global version of an atmospheric quasi-equilibrium tropical circulation model (Neelin and Zeng, 2000; Zeng et al., 2000), a simple land model (Zeng et al., 2000), and a slab mixed layer ocean model with Q flux to represent the effects of ocean dynamics (Hansen et al., 1984). The mixed layer ocean depth is the annual mean derived from Levitus et al. (2000). All models are run at $5.6° \times 3.7°$ horizontal resolution, limited by the atmospheric component. The terrestrial carbon model VEGAS (Zeng, 2003; Zeng et al., 2004, 2005) is a dynamic vegetation model with full soil carbon dynamics. Competition among four plant functional types is determined by climatic constraints and resource allocation strategy such as temperature tolerance and height-dependent shading. Phenology is simulated dynamically as the balance between growth and respiration/turnover, so whether a plant functional type is deciduous or evergreen is interactively determined. There are six soil carbon pools with varying temperature dependence of respiration: microbial, metabolic and structural litter; fast, intermediate, and slow soil. A three-box ocean carbon model including low latitude, high latitude, and deep ocean (Archer et al., 2000) is coupled to the terrestrial component through a fully mixed atmosphere. No ocean biology or sea ice is included in the model.

– *UV*: The UVic ESCM version 2.9 (Weaver et al., 2001; Eby et al., 2009) consists of a primitive equation, 3-D ocean general circulation model coupled to a dynamic–thermodynamic sea-ice model and an atmospheric energy–moisture balance model with dynamical feedbacks (Weaver et al., 2001). The model conserves heat, moisture, and carbon between components to machine precision without flux adjustments. The land surface and terrestrial vegetation components are represented by a simplified version of the Hadley Centre's MOSES land-surface scheme coupled to the dynamic vegetation model TRIFFID (Meissner et al., 2003). Land carbon fluxes are calculated within MOSES and are allocated to vegetation and soil carbon pools (Matthews et al., 2004). Ocean carbon is simulated by means of an OCMIP-type inorganic carbon-cycle model and a NPZD marine ecosystem model with two nutrients (PO_4 and NO_3), two phytoplankton classes, and prognostic denitrification (Schmittner et al., 2008). Sediment processes are represented using an oxic-only model of sediment respiration (Archer, 1996). Terrestrial weathering is diagnosed from the net sediment flux during spin-up and held fixed at the equilibrium pre-industrial value for transient simulations. The model was spun up with boundary conditions from the year 1800 for more than 10 000 yr.

Appendix B

Forcing descriptions

The recommended externally specified forcings for the historical simulations follow the PMIP3 last millennium and CMIP5 RCP experimental protocols. Unlike the PMIP3 protocol only one forcing dataset was recommended. Models that were not able to incorporate the recommended forcing were encouraged to use the equivalent radiative forcing estimates from the Task Group: RCP Concentrations Calculation and Data (Meinshausen et al., 2011).

The recommended forcings were applied over the last millennium for the appropriate individually forced and all-forcing simulations. Since most EMICs are not able to simulate the warming from black carbon, the indirect effect of ozone, or the cooling from the indirect effect of sulphate aerosols, these forcings were excluded. The excluded forcings are all highly uncertain and in general tend to cancel out, and so no extra net external forcing was specified in order to compensate for their exclusion (Meinshausen et al., 2011). A description of the recommended forcing and any model deviations from the experimental protocol are as follows.

- *CO_2 forcing* is from the recommended PMIP3 (years 850 to 1800) and the CMIP5 RCP (years 1765 to 2005) historical CO_2 concentrations (Schmidt et al., 2012; Meinshausen et al., 2011). The annual mean values were linearly blended between years 1765 and 1800 and converted to radiative forcing as in the AR4 (Forster et al., 2007). All models applied this forcing through changes in their radiative transfer schemes. Individual modelling groups supplied their own estimates of any emissions needed for the free CO_2 experiments.

- *Land-use forcing* is from the recommended PMIP3 data of Pongratz et al. (2008), between years 850 and 1699, and the CMIP5 historical RCP land-use dataset of Hurtt et al. (2011), between years 1500 and 2005. Only the changes in the annual mean area of crop and pasture were used. The datasets were linearly blended between years 1500 and 1699. The B3, DC, GE, I2, and UV models apply the forcing through changes in the local surface albedo, hydrology and as internally calculated carbon fluxes due to vegetation cover changes. The IA and LO model applied land-use forcing only as changes in surface albedo and hydrology. Only the equivalent radiative forcing from the Task Group: RCP Concentrations Calculation and Data, due to albedo changes, was applied as a change in net top-of-atmosphere (TOA) shortwave radiation by the C2, C3, MI, ME and UM models.

- *Non-CO_2 greenhouse gas forcing* is from the recommended PMIP3 (years 850 to 1800) and the CMIP5 (years 1765 to 2005) historical RCP non-CO_2 greenhouse gas concentrations (Schmidt et al., 2012; Meinshausen et al., 2011) converted to an aggregated radiative forcing as in the AR4 (Forster et al., 2007). The annual mean data were linearly blended between 1765 and 1800. All models applied non-CO_2 greenhouse gas forcing through changes in their radiative transfer schemes.

- *Orbital forcing* followed Berger (1978) and changed only between years 850 and 2005. Orbital parameters are fixed at their year 2005 values, after 2005. Orbital changes are applied as changes in the TOA incoming solar radiation. The IA, ME and UM models did not include changes in orbital forcing in any simulations.

- *Solar irradiance forcing* is from the PMIP3 recommended datasets of Delaygue and Bard (2009), between years 850 and 1609, and the CMIP5 forcing of Wang et al. (2005), between years 1610 and 2008. These datasets include annual variation from both the solar cycle and background solar irradiance. Since the solar irradiance from Wang et al. (2005) dataset is very close to that from Delaygue and Bard (2009) at year 1610, the datasets were spliced at this year. The spin-up used a constant average of the first solar cycle (after year 850) of $1365.76\,W\,m^{-2}$. After year 2008, a repeating solar cycle 23 was added. All models applied changes in solar irradiance as changes in incoming shortwave.

- *Sulphate aerosol forcing* is from the CMIP5 historical RCP SO_4 concentration data (Lamarque et al., 2010) converted to optical depth. SO_4 concentrations are vertically integrated to determine the atmospheric sulphate aerosol burden ($g\,m^{-2}$). The burden is then multiplied by a constant specific extinction cross-section factor of $8\,m^2\,g^{-1}$ to obtain the optical depth. Only the direct effect of sulphate forcing was to be included. The data are monthly, from January 1855 to December 2105. The B3, IA, I2, LO and UV models calculated the forcing internally from a change in surface albedo. The equivalent radiative forcing from the Task Group: RCP Concentrations Calculation and Data, due to albedo changes, was applied as a change in the net TOA shortwave radiation by the C2, C3, GE, MI and UM models. The GE model applies the equivalent radiative forcing as a perturbation to the outgoing longwave. The UM model specified the direct and indirect effects of sulphates while the ME model did not include any sulphate forcing.

- *Volcanic forcing* is from the PMIP-recommended Crowley et al. (2008) dataset. For most models aerosol optical depth (AOD) was globally averaged and converted to radiative forcing (RF) and applied as a reduction in net TOA shortwave. A simple linear conversion constant of -20 is used to convert AOD to RF for negative forcing less than $1.5\,W\,m^{-2}$ and 2/3 of this conversion constant for the portion of the negative forcing greater than $1.5\,W\,m^{-2}$. The smaller conversion constant effectively reduces the radiative forcing for large eruptions. Peak forcing for the Tambora eruption is reduced to about $6\,W\,m^{-2}$ as in Crowley (2000), but peak forcing for Krakatoa and Pinatubo is kept near the $3\,W\,m^{-2}$ estimated in the AR4. This dataset has approximately 10-day temporal resolution for the years 850 to 1998. This forcing has been made into an anomaly with a positive radiative forcing of approximately $0.207\,W\,m^{-2}$, when there was no negative volcanic forcing. Anomalous volcanic forcing during the spin-up, and after 1998, was set

to zero. The GE model applies volcanic radiative forcing as a perturbation to the outgoing longwave. The ML model used equivalent radiative forcing from the Task Group: RCP Concentrations Calculation and Data. All models specified volcanic forcing.

Acknowledgements. A. J. W., M. E. and K. A. are grateful for ongoing support from NSERC through its Discovery Grant, G8 and CREATE programs. TF and EC acknowledge support from the Belgian Federal Science Policy Office. N. R. E. and P. B. H. acknowledge support from EU FP7 ERMITAGE grant no. 265170. H. G. is Senior Research Associate with the Fonds National de la Recherche Scientifique (F.R.S. – FNRS-Belgium). We also acknowledge the World Climate Research Programme's Working Group on Coupled Modelling, which is responsible for CMIP, and we thank the climate modelling groups (bcc-csm1-1, CCSM4, FGOALS-gl, GISS-E2-R, IPSL-CM5A-LR, MIROC-ESM, MPI-ESM-P) for producing and making available their model output. For CMIP the US Department of Energy's Program for Climate Model Diagnosis and Intercomparison provides coordinating support and led development of software infrastructure in partnership with the Global Organization for Earth System Science Portals.

Edited by: M. Kageyama

References

Andrews, T., Gregory, J. M. , Webb, M. J., and Taylor, K. E.: Forcing, Feedbacks and Climate Sensitivity in CMIP5 Coupled Atmosphere-Ocean Climate Models, Geophys. Res. Lett., 39, L09712, doi:10.1029/2012GL051607, 2012.

Annan, J. D. and Hargreaves, J. C.: Efficient identification of ocean thermodynamics in a physical/biogeochemical ocean model with an iterative Importance Sampling method, Ocean Model., 32, 205–215, doi:10.1016/j.ocemod.2010.02.003, 2010.

Archer, D.: A data-driven model of the global calcite lysocline, Global Biogeochem. Cy., 10, 511–526, doi:10.1029/96GB01521, 1996.

Archer, D. E., Eshel, G., Winguth, A., Broecker, W., Pierrehumbert, R., Tobis, M., and Jacob, R.: Atmospheric pCO_2 sensitivity to the biological pump in the ocean, Global Biogeochem. Cy., 14, 1219–1230, doi:10.1029/1999GB001216, 2000.

Archer, D., Eby, M., Brovkin, V., Ridgwell, A., Cao, L., Mikolajewicz, U., Caldeira, K., Matsumoto, K., Munhoven, G., Montenegro, A., and Tokos, K.: Atmospheric Lifetime of Fossil Fuel Carbon Dioxide, Annu. Rev. Earth Planet. Sci., 37, 117–134, 2009.

Arzhanov, M. M., Demchenko, P. F., Eliseev, A. V., and Mokhov, I. I.: Simulation of characteristics of thermal and hydrologic soil regimes in equilibrium numerical experiments with a climate model of intermediate complexity, Izv. Atmos. Ocean. Phys., 44, 548–566, doi:10.1134/S0001433808050022, 2008.

Berger, A. L.: Long-term variations of daily insolation and quaternary climatic changes, J. Atmos. Sci., 35, 2362–2367, doi:10.1175/1520-0469(1978)035<2362:LTVODI>2.0.CO;2, 1978.

Boden, T. A., Marland, G., and Andres, R. J.: Global, Regional, and National Fossil-Fuel CO_2 Emissions, Carbon Dioxide Information Analysis Center, Oak Ridge National Laboratory, US Department of Energy, Oak Ridge, Tenn., USA,doi:10.3334/CDIAC/00001_V2012, 2012.

Brovkin, V., Bendtsen, J., Claussen, M., Ganopolski, A., Kubatzki, C., Petoukhov, V., and Andreev, A.: Carbon cycle, vegetation and climate dynamics in the Holocene: Experiments with the CLIMBER-2 model, Global Biogeochem. Cy., 16, 1139–1159, doi:10.1029/2001GB001662, 2002.

Brovkin, V., Claussen, M., Driesschaert, E., Fichefet, T., Kicklighter, D., Loutre, M. F., Matthews, H. D., Ramankutty, N., Schaeffer, M., and Sokolov, A.: Biogeophysical effects of historical land cover changes simulated by six Earth system models of intermediate complexity, Clim. Dynam., 26, 587–600, 2006.

Calov, R., Ganopolski, A., Petoukhov, V., Claussen, M., and Greve, R.: Large-scale instabilities of the Laurentide ice sheet simulated in a fully coupled climate-system model, Geophys. Res. Lett., 29, 2216–2218, doi:10.1029/2002GL016078, 2002.

Cimatoribus, A. A., Drijfhout, S. S., and Dijkstra, H. A.: A global hybrid coupled model based on Atmosphere-SST feedbacks, Clim. Dynam., 38, 745–760, doi:10.1007/s00382-011-1094-1, 2012.

Claussen, M., Mysak, L. A., Weaver, A. J., Crucifix, M., Fichefet, T., Loutre, M.-F., Weber, S. L., Alcamo, J., Alexeev, V. A., Berger, A., Calov, R., Ganopolski, A., Goosse, H., Lohmann, G., Lunkeit, F., Mokhov, I. I., Petoukhov, V., Stone, P., and Wang, Z.: Earth system models of intermediate complexity: closing the gap in the spectrum of climate system models, Clim. Dynam., 18, 579–586, doi:10.1007/s00382-001-0200-1, 2002.

Cox, M. D.: GFDL Ocean Group Technical Report 1: A primitive equation, 3-dimensional model of the ocean, NOAA/GFDL, Princeton, USA, 1984.

Cox, P. M.: Description of the "TRIFFID" Dynamic Global Vegetation Model, Technical Note 24, Hadley Centre, Bracknell, UK, 2001.

Cox, P. M., Betts, R. A., Bunton, C. B., Essery, R. L. H., Rowntree, P. R., and Smith, J.: The impact of new land surface physics on the GCM simulation of climate and climate sensitivity, Clim. Dynam., 15, 183–203, doi:10.1007/s003820050276, 1999.

Crowley, T. J.: Causes of climate change over the past 1000 years, Science, 289, 270–277, 2000.

Crowley, T. J., Zielinski, G., Vinther, B., Udisti, R., Kreutz, K., Cole-Dai, J., and Castellano, E.: Volcanism and the Little Ice Age, PAGES News, 16, 22–23, 2008.

Delaygue, G. and Bard, E.: Solar forcing based on ^{10}Be in Antarctica ice over the past millennium and beyond, Geophys. Res. Abstr., 11, EGU2009-6943, 2009.

Denman, K. L., Brasseur, G., Chidthaisong, A., Ciais, P., Cox, P. M., Dickinson, R. E., Hauglustaine, D., Heinze, C., Holland, E., Jacob, D., Lohmann, U., Ramachandran, S., da Silva Dias, P. L., Wofsy, S. C., and Zhang, X.: Couplings between changes in the climate system and biogeochemistry, in: Climate Change 2007: The Physical Science Basis, Contribution of Working Group I to the Fourth Assessment Report of the Intergovernmental Panel on Climate Change, edited by: Solomon, S., Qin, D., Manning, M., Chen, Z., Marquis, M., Averyt, K. B., Tignor, M., and Miller, H. L., Cambridge University Press, Cambridge, UK and New York, USA, 2007.

Eby, M., Zickfeld, K., Montenegro, A., Archer, D., Meissner, K. J., and Weaver, A. J.: Lifetime of anthropogenic climate

change: millennial time scales of potential CO_2 and surface temperature perturbations, J. Climate, 22, 2501–2511, doi:10.1175/2008JCLI2554.1, 2009.

Edwards, N. R. and Marsh, R.: Uncertainties due to transport-parameter sensitivity in an efficient 3-D ocean-climate model, Clim. Dynam., 24, 415–433, doi:10.1007/s00382-004-0508-8, 2005.

Edwards, N. R., Willmott, A. J., and Killworth, P. D.: On the role of topography and wind stress on the stability of the thermohaline circulation, J. Phys. Oceanogr., 28, 756–778, doi:10.1175/1520-0485(1998)028<0756:OTROTA>2.0.CO;2, 1998.

Eliseev, A. V. and Mokhov, I. I.: Uncertainty of climate response to natural and anthropogenic forcings due to different land use scenarios, Adv. Atmos. Sci., 28, 1215–1232, doi:10.1007/s00376-010-0054-8, 2011.

Fanning, A. F. and Weaver, A. J.: An atmospheric energy-moisture balance model: climatology, interpentadal climate change, and coupling to an ocean general circulation model, J. Geophys. Res., 101, 15111–15128, doi:10.1029/96JD01017, 1996.

Farquhar, G. D., Caemmerer, S. V., and Berry, J. A.: A biochemical model of photosynthetic CO_2 assimilation in leaves of C-3 species, Planta, 149, 78–90, doi:10.1007/BF00386231, 1980.

Felzer, B., Kicklighter, D., Melillo, J., Wang, C., Zhuang, Q., and Prinn, R.: Effects of ozone on net primary production and carbon sequestration in the conterminous United States using a biogeochemistry model, Tellus B, 56, 230–248, doi:10.1111/j.1600-0889.2004.00097.x, 2004.

Fernández-Donado, L., González-Rouco, J. F., Raible, C. C., Ammann, C. M., Barriopedro, D., García-Bustamante, E., Jungclaus, J. H., Lorenz, S. J., Luterbacher, J., Phipps, S. J., Servonnat, J., Swingedouw, D., Tett, S. F. B., Wagner, S., Yiou, P., and Zorita, E.: Large-scale temperature response to external forcing in simulations and reconstructions of the last millennium, Clim. Past, 9, 393–421, doi:10.5194/cp-9-393-2013, 2013.

Feulner, G.: Are the most recent estimates for Maunder Minimum solar irradiance in agreement with temperature reconstructions?, Geophys. Res. Lett., 38, L16706, doi:10.1029/2011GL048529, 2011

Fichefet, T. and Morales Maqueda, M. A.: Sensitivity of a global sea ice model to the treatment of ice thermodynamics and dynamics, J. Geophys. Res., 102, 12609–12646, 1997.

Forster, P., Ramaswamy, V., Artaxo, P., Berntsen, T., Betts, R., Fahey, D. W., Haywood, J., Lean, J., Lowe, D. C., Myhre, G., Nganga, J., Prinn, R., Raga, G., Schulz, M., and Van Dorland, R.: Changes in Atmospheric Constituents and in Radiative Forcing, in: Climate Change 2007: The Physical Science Basis, Contribution of Working Group I to the Fourth Assessment Report of the Intergovernmental Panel on Climate Change, edited by: Solomon, S., Qin, D., Manning, M., Chen, Z., Marquis, M., Averyt, K. B., Tignor, M., and Miller, H. L., Cambridge University Press, Cambridge, UK and New York, USA, 2007.

Frank, D. C., Esper, J., Raible, C. C., Büntgen, U., Trouet, V., Stocker, B., and Joos, F.: Ensemble reconstruction constraints on the global carbon cycle sensitivity to climate, Nature, 463, 527–530, doi:10.1038/nature08769, 2010.

Friedlingstein, P., Cox, P., Betts, R., Bopp, L., von Bloh, W., Brovkin, V., Cadule, P., Doney, S., Eby, M., Fung, I., Bala, G., John, J., Jones, C., Joos, F., Kato, T., Kawamiya, M., Knorr, W., Lindsay, K., Matthews, H. D., Raddatz, T., Payner, P., Reick, C., Roeckner, E., Schnitzler, K.-G., Schnur, R., Strassman, K., Weaver, A. J., Yoshikawa, C., and Zeng, N.: Climate-carbon cycle feedback analysis: results from the C^4MIP model intercomparison, J. Climate, 19, 3337–3353, doi:10.1175/JCLI3800.1, 2006.

Fyke, J. G., Weaver, A. J., Pollard, D., Eby, M., Carter, L., and Mackintosh, A.: A new coupled ice sheet/climate model: description and sensitivity to model physics under Eemian, Last Glacial Maximum, late Holocene and modern climate conditions, Geosci. Model Dev., 4, 117–136, doi:10.5194/gmd-4-117-2011, 2011.

Gangstø, R., Joos, F., and Gehlen, M.: Sensitivity of pelagic calcification to ocean acidification, Biogeosciences, 8, 433–458, doi:10.5194/bg-8-433-2011, 2011.

Ganopolski, A., Petoukhov, V., Rahmstorf, S., Brovkin, V., Claussen, M., Eliseev, A., and Kubatzki, C.: CLIMBER-2: a climate system model of intermediate complexity, Part II: model sensitivity, Clim. Dynam., 17, 735–751, doi:10.1007/s003820000144, 2001.

Gehlen, M., Bopp, L., Emprin, N., Aumont, O., Heinze, C., and Ragueneau, O.: Reconciling surface ocean productivity, export fluxes and sediment composition in a global biogeochemical ocean model, Biogeosciences, 3, 521–537, doi:10.5194/bg-3-521-2006, 2006

Gerber, S., Joos, F., Brügger, P., Stocker, T., Mann, M., Sitch, S., and Scholze, M.: Constraining temperature variations over the last millennium by comparing simulated and observed atmospheric CO_2, Clim. Dynam., 20, 281–299, doi:10.1007/s00382-002-0270-8, 2003.

Gerten, D., Schaphoff, S., Haberlandt, U., Lucht, W., and Sitch, S.: Terrestrial vegetation and water balance – hydrological evaluation of a dynamic global vegetation model, J. Hydrol., 286, 249–270, doi:10.1016/j.jhydrol.2003.09.029, 2004.

González-Rouco, F., Von Storch, H., and Zorita, E.: Deep soil temperature as proxy for surface air-temperature in a coupled model simulation of the last thousand years, Geophys. Res. Lett., 30, 2116, doi:10.1029/2003GL018264, 2003.

Goosse, H. and Fichefet, T.: Importance of ice-ocean interactions for the global ocean circulation: A model study, J. Geophys. Res., 104, 23337–23355, 1999.

Goosse, H., Brovkin, V., Fichefet, T., Haarsma, R., Huybrechts, P., Jongma, J., Mouchet, A., Selten, F., Barriat, P.-Y., Campin, J.-M., Deleersnijder, E., Driesschaert, E., Goelzer, H., Janssens, I., Loutre, M.-F., Morales Maqueda, M. A., Opsteegh, T., Mathieu, P.-P., Munhoven, G., Pettersson, E. J., Renssen, H., Roche, D. M., Schaeffer, M., Tartinville, B., Timmermann, A., and Weber, S. L.: Description of the Earth system model of intermediate complexity LOVECLIM version 1.2, Geosci. Model Dev., 3, 603–633, doi:10.5194/gmd-3-603-2010, 2010.

Goosse, H., Crespin, E., Dubinkina, S., Loutre, M.-F., Mann, M. E., Renssen, H., Sallaz-Damaz, Y., and Shindell, D.: The role of forcing and internal dynamics in explaining the "Medieval Climate Anomaly", Clim Dynam., 39, 2847–2866, doi:10.1007/s00382-012-1297-0, 2012.

Gordon, C., Cooper, C., Senior, C. A., Banks, H., Gregory, J. M., Johns, T. C., Mitchell, J. F. B., and Wood, R. A.: The simulation of SST, sea ice extents and ocean heat transports in a version of the Hadley Centre coupled model without flux adjustments, Clim. Dynam., 16, 147–168, doi:10.1007/s003820050010, 2000.

Gregory, J. M., Dixon, K. W., Stouffer, R. J., Weaver, A. J., Driesschaert, E., Eby, M., Fichefet, T., Hasumi, H., Hu, A., Jungclaus, J. H., Kamenkovich, I. V., Levermann, A., Montoya, M., Murakami, S., Nawrath, S., Oka, A., Sokolov, A. P., and Thorpe, R. B.: A model intercomparison of changes in the Atlantic thermohaline circulation in response to increasing atmospheric CO_2 concentration, Geophys. Res. Lett., 32, L12703, doi:10.1029/2005GL023209, 2005.

Gregory, J. M., Jones, C. D., Cadule, P., and Friedlingstein, P.: Quantifying carbon cycle feedbacks, J. Climate, 22, 5232–5250, doi:10.1175/2009JCLI2949.1, 2009.

Hansen, J., Lacis, A., Rind, D., Russell, G., Stone, P., Fung, I., Ruedy, R., and Lerner, J.: Climate sensitivity: analysis of feedback mechanisms, in: Climate Processes and Climate Sensitivity, AGU Geophysical Monograph 29, edited by: Hansen, J. E. and Takahashi, T., AGU, 1984.

Hasumi, H.: CCSR Ocean Component Model (COCO) Version 4.0, CCSR Report No. 25, Centre for Climate System Research, University of Tokyo, Japan, 2006.

Hasumi, H. and Emori, S.: K-1 coupled GCM (MIROC) description, K-1 Technical Report No. 1, Center for Climate System Research, University of Tokyo, Japan, 2004.

Hegerl, G. C., Zwiers, F. W., Braconnot, P., Gillett, N. P., Luo, Y., Marengo Orsini, J. A., Nicholls, N., Penner, J. E., and Stott, P. A.: Understanding and Attributing Climate Change, in: Climate Change 2007: The Physical Science Basis, Contribution of Working Group I to the Fourth Assessment Report of the Intergovernmental Panel on Climate Change, edited by: Solomon, S., Qin, D., Manning, M., Chen, Z., Marquis, M., Averyt, K. B., Tignor, M., and Miller, H. L., Cambridge University Press, Cambridge, UK and New York, USA, 2007.

Heinze, C., Maier-Reimer, E., Winguth, A. M. E., and Archer, D.: A global oceanic sediment model for long-term climate studies, Global Biogeochem. Cy., 13, 221–250, doi:10.1029/98GB02812, 1999.

Hofmann, M. and Morales Maqueda, M. A.: Performance of a second-order moments advection scheme in an Ocean General Circulation Model, J. Geophys. Res., 111, C05006, doi:10.1029/2005JC003279, 2006.

Holden, P. B., Edwards, N. R., Gerten, D., and Schaphoff, S.: A model-based constraint on CO_2 fertilisation, Biogeosciences, 10, 339–355, doi:10.5194/bg-10-339-2013, 2013.

Holian, G. L., Sokolov, A. P., and Prinn, R. G.: Uncertainty in atmospheric CO_2 predictions from a global ocean carbon cycle model, Report 80, MIT Joint Program on the Science and Policy of Global Change, Cambridge, USA, 2001.

Houghton, R. A.: Carbon Flux to the Atmosphere from Land-Use Changes: 1850–2005, in: TRENDS: A Compendium of Data on Global Change, Carbon Dioxide Information Analysis Center, Oak Ridge National Laboratory, US Department of Energy, Oak Ridge, Tenn., USA, 2008.

Hurtt, G. C., Chini, L. P., Frolking, S., Betts, R. A., Feddema, J., Fischer, G., Fisk, J. P., Hibbard, K., Houghton, R. A., Janetos, A., Jones, C. D., Kindermann, G., Kinoshita, T., Klein Goldewijk, K., Riahi, K., Shevliakova, E., Smith, S., Stehfest, E., Thomson, A., Thornton, P., van Vuuren, D. P., and Wang, Y. P.: Harmonization of land-use scenarios for the period 1500–2100: 600 years of global gridded annual land-use transitions, wood harvest, and resulting secondary lands, Climatic Change, 109, 117–161, doi:10.1007/s10584-011-0153-2, 2011.

Huybrechts, P.: Sea-level changes at the LGM from ice-dynamic reconstructions of the Greenland and Antarctic ice sheets during the glacial cycles, Quaternary Sci. Rev., 21, 203–231, doi:10.1016/S0277-3791(01)00082-8, 2002.

IPCC: Climate Change 2007: The Physical Science Basis, in: Contribution of Working Group I to the Fourth Assessment Report of the Intergovernmental Panel on Climate Change, edited by: Solomon, S., Qin, D., Manning, M., Chen, Z., Marquis, M., Averyt, K. B., Tignor, M., and Miller, H. L., Cambridge University Press, Cambridge, UK and New York, USA, 2007.

Ito, A., and Oikawa, T: A simulation model of the carbon cycle in land ecosystems (Sim-CYCLE): a description based on dry-matter production theory and plot-scale validation, Ecol. Model., 151, 143–176, doi:10.1016/S0304-3800(01)00473-2, 2002.

Jones, C., Gregory, J., Thorpe, R., Cox, P., Murphy, J., Sexton, D., and Valdes, P.: Systematic optimisation and climate simulation of FAMOUS, a fast version of HadCM3, Clim. Dynam., 25, 189–204, doi:10.1007/s00382-005-0027-2, 2005.

Jones, P. D., New, M., Parker, D. E., Martin, S., and Rigor, I. G.: Surface air temperature and its changes over the past 150 years, Rev. Geophys., 37, 173–199, doi:10.1029/1999RG900002, 1999.

Joos, F., Prentice, I. C., Sitch, S., Meyer, R., Hooss, G., Plattner, G.-K., Gerber, S., and Hasselmann, K.: Global warming feedbacks on terrestrial carbon uptake under the Intergovernmental Panel on Climate Change (IPCC) Emission Scenarios, Global Biogeochem. Cy., 15, 891–907, doi:10.1029/2000GB001375, 2001.

Joos, F., Roth, R., Fuglestvedt, J. S., Peters, G. P., Enting, I. G., von Bloh, W., Brovkin, V., Burke, E. J., Eby, M., Edwards, N. R., Friedrich, T., Frölicher, T. L., Halloran, P. R., Holden, P. B., Jones, C., Kleinen, T., Mackenzie, F. T., Matsumoto, K., Meinshausen, M., Plattner, G.-K., Reisinger, A., Segschneider, J., Shaffer, G., Steinacher, M., Strassmann, K., Tanaka, K., Timmermann, A., and Weaver, A. J.: Carbon dioxide and climate impulse response functions for the computation of greenhouse gas metrics: a multi-model analysis, Atmos. Chem. Phys., 13, 2793–2825, doi:10.5194/acp-13-2793-2013, 2013.

Jungclaus, J. H., Lorenz, S. J., Timmreck, C., Reick, C. H., Brovkin, V., Six, K., Segschneider, J., Giorgetta, M. A., Crowley, T. J., Pongratz, J., Krivova, N. A., Vieira, L. E., Solanki, S. K., Klocke, D., Botzet, M., Esch, M., Gayler, V., Haak, H., Raddatz, T. J., Roeckner, E., Schnur, R., Widmann, H., Claussen, M., Stevens, B., and Marotzke, J.: Climate and carbon-cycle variability over the last millennium, Clim. Past, 6, 723–737, doi:10.5194/cp-6-723-2010, 2010.

Kaplan, J. O., Krumhardt, K., Ellis, E. C., and Ruddiman, W. F.: Holocene carbon emissions as a result of anthropogenic land cover change, Holocene, 21, 775–791, doi:10.1177/0959683610386983, 2010.

Kucharski, F. and Molteni, F.: On non-linearities in a forced North Atlantic Oscillation, Clim. Dynam., 21, 677–687, doi:10.1007/s00382-003-0347-z, 2003.

Lamarque, J.-F., Bond, T. C., Eyring, V., Granier, C., Heil, A., Klimont, Z., Lee, D., Liousse, C., Mieville, A., Owen, B., Schultz, M. G., Shindell, D., Smith, S. J., Stehfest, E., Van Aardenne, J., Cooper, O. R., Kainuma, M., Mahowald, N., McConnell, J. R., Naik, V., Riahi, K., and van Vuuren, D. P.: Historical (1850–2000) gridded anthropogenic and biomass burning emissions of reactive gases and aerosols: methodology and ap-

plication, Atmos. Chem. Phys., 10, 7017–7039, doi:10.5194/acp-10-7017-2010, 2010.

Latif, M., Böning, C., Willebrand, J., Biastoch, A., Dengg, J., Keenlyside, N., and Schweckendiek, U.: Is the thermohaline circulation changing?, J. Climate, 19, 4631–4637, doi:10.1175/JCLI3876.1, 2006.

Levitus, S., Antonov, J., Boyer, T. P., and Stephens, C.: Warming of the world ocean, Science, 287, 2225–2229, doi:10.1126/science.287.5461.2225, 2000.

Levitus, S., Antonov, J. I., Boyer, T. P., Baranova, O. K., Garcia, H. E., Locarnini, R. A., Mishonov, A. V., Reagan, J. R., Seidov, D., Yarosh, E. S., and Zweng, M. M.: World ocean heat content and thermosteric sea level change (0–2000 m), 1955–2010, Geophys. Res. Lett., 39, L10603, doi:10.1029/2012GL051106, 2012.

Liu, Y.: Modeling the emissions of nitrous oxide and methane from the terrestrial biosphere to the atmosphere, Report 10, MIT Joint Program on the Science and Policy of Global Change, Cambridge, USA, 1996.

Maier-Reimer, E. and Hasselmann, K.: Transport and storage of CO_2 in the ocean – an inorganic ocean-circu1ation carbon cycle model, Clim. Dynam., 2, 63–90, 1987.

Mann, M., Zhang, Z., Hughes, M., Bradley, R., Miller, S., Rutherford, S., and Ni, F.: Proxy-based reconstructions of hemispheric and global surface temperature variations over the past two millennia, P. Natl. Acad. Sci. USA, 105, 13252–13257, doi:10.1073/pnas.0805721105, 2008.

Mann, M. E., Fuentes, J. D., and Rutherford, S.: Underestimation of volcanic cooling in tree-ring-based reconstructions of hemispheric temperatures, Nat. Geosci., 5, 202–205, doi:10.1038/NGEO1394, 2012.

Marsh, R., Müller, S. A., Yool, A., and Edwards, N. R.: Incorporation of the C-GOLDSTEIN efficient climate model into the GENIE framework: "eb_go_gs" configurations of GENIE, Geosci. Model Dev., 4, 957–992, doi:10.5194/gmd-4-957-2011, 2011.

Matsumoto, K., Tokos, K. S., Price, A. R., and Cox, S. J.: First description of the Minnesota Earth System Model for Ocean biogeochemistry (MESMO 1.0), Geosci. Model Dev., 1, 1–15, doi:10.5194/gmd-1-1-2008, 2008.

Matthews, H. D., Weaver, A. J., Meissner, K. J., Gillett, N. P., and Eby, M.: Natural and anthropogenic climate change: incorporating historical land cover change, vegetation dynamics and the global carbon cycle, Clim. Dynam., 22, 461–479, doi:10.1007/s00382-004-0392-2, 2004.

Matthews, H. D., Gillett, N. P., Stott, P. A., and Zickfeld, K.: The proportionality of global warming to cumulative carbon emissions, Nature, 459, 829–832, doi:10.1038/nature08047, 2009.

Meinshausen, M., Smith, S. J., Calvin, K. V., Daniel, J. S., Kainuma, M. L. T., Lamarque, J.-F., Matsumoto, K., Montzka, S. A., Raper, S. C. B., Riahi, K., Thomson, A. M., Velders, G. J. M., and van Vuuren, D. P.: The RCP Greenhouse Gas Concentrations and their Extension from 1765 to 2300, Climatic Change, 109, 213–241, doi:10.1007/s10584-011-0156-z, 2011.

Meissner, K. J., Weaver, A. J., Matthews, H. D., and Cox, P. M.: The role of land surface dynamics in glacial inception: a study with the UVic Earth System model, Clim. Dynam., 21, 515–537, doi:10.1007/s00382-003-0352-2, 2003.

Melillo, J. M., McGuire, A. D., Kicklighter, D. W., Moore, B., Vorosmarty, C. J., and Schloss, A. L.: Global climate change and terrestrial net primary production, Nature, 363, 234–240, doi:10.1038/363234a0, 1993.

Miller, G. H., Geirsdóttir, A., Zhong, Y., Larsen, D. J., Otto-Bliesner, B. L., Holland, M., Bailey, D. A., Refsnider, K. A., Lehman, S. J., Southon, J. R., Anderson, C., Björnsson, H., and Thordarson, T.: Abrupt onset of the Little Ice Age triggered by volcanism and sustained by sea-ice/ocean feedbacks, Geophys. Res. Lett., 39, L02708, doi:10.1029/2011GL050168, 2012.

Mitchell, L., Brook, E., Sowers, T., McConnell, J., and Taylor, K.: Multidecadal variability of atmospheric methane, 1000–1800 CE, J. Geophys. Res.-Biogeo., 116, G02007, doi:10.1029/2010jg001441, 2011.

Molteni, F.: Atmospheric simulations using a GCM with simplified physical parameterizations, I: model climatology and variability in multi-decadal experiments, Clim. Dynam., 20, 175–191, doi:10.1007/s00382-002-0268-2, 2003.

Montoya, M., Griesel, A., Levermann, A., Mignot, J., Hofmann, M., Ganopolski, A., and Rahmstorf, S.: The earth system model of intermediate complexity CLIMBER-3α, Part I: description and performance for present-day conditions, Clim. Dynam., 26, 327—328, doi:10.1007/s00382-005-0061-0, 2006.

Morice, C. P., Kennedy, J. J., Rayner, N. A., and Jones, P. D.: Quantifying uncertainties in global and regional temperature change using an ensemble of observational estimates: The HadCRUT4 data set, J. Geophys. Res., 117, D08101, doi:10.1029/2011JD017187, 2012.

Mouchet, A. and François, L. M.: Sensitivity of a global oceanic carbon cycle model to the circulation and the fate of organic matter: preliminary results, Phys. Chem. Earth, 21, 511–516, 1996.

Müller, S. A., Joos, F., Edwards, N. R., and Stocker, T. F.: Water mass distribution and ventilation time scales in a cost-efficient, three-dimensional ocean model, J. Climate, 19, 5479–5499, doi:10.1175/JCLI3911.1, 2006.

Muryshev, K. E., Eliseev, A. V., Mokhov, I. I., and Diansky, N. A.: Validating and assessing the sensitivity of the climate model with an ocean general circulation model developed at the Institute of Atmospheric Physics, Russian Academy of Sciences, Izv. Atmos. Ocean. Phys., 45, 416–433, doi:10.1134/S0001433809040033, 2009.

Myhre, G., Highwood, E. J., Shine, K. P., and Stordal, F.: New estimates of radiative forcing due to well mixed greenhouse gases, Geophys. Res. Lett., 25, 2715–2718, doi:10.1029/98GL01908, 1998.

Najjar, R. G. and Orr, J. C.: Biotic-HOWTO, OCMIP internal report, LSCE/CEA Saclay, Gif-sur-Yvette, France, 1999.

Neelin, J. D. and Zeng, N.: A quasi-equilibrium tropical circulation model – formulation, J. Atmos. Sci., 57, 1741–1766, doi:10.1175/1520-0469(2000)057<1741:AQETCM>2.0.CO;2, 2000.

Oka, A., Tajika, E., Abe-Ouchi, A., and Kubota, K.: Role of the ocean in controlling atmospheric CO_2 concentration in the course of global glaciations, Clim. Dynam., 37, 1755–1770, doi:10.1007/s00382-010-0959-z, 2011.

Oleson, K. W., Niu, G.-Y., Yang, Z.-L., Lawrence, D. M., Thornton, P. E., Lawrence, P. J., Stöckli, R., Dickinson, R. E., Bonan, G. B., Levis, S., Dai, A., and Qian, T.: Improvements to the Community Land Model and their impact on the hydrological cycle, J. Geophys. Res., 113, G01021, doi:10.1029/2007JG000563, 2008.

Opsteegh, J. D., Haarsma, R. J., Selten, F. M., and Kattenberg, A.: ECBILT: a dynamic alternative to mixed boundary conditions

in ocean models, Tellus A, 50, 348–367, doi:10.1034/j.1600-0870.1998.t01-1-00007.x, 1998.

Orr, J., Najjar, R., Sabine, C., and Joos, F.: Abiotic-HOWTO, OCMIP internal report, LSCE/CEA Saclay, Gif-sur-Yvette, France, 2000.

Pacanowski, R. C. and Griffes, S. M.: The MOM3 Manual, NOAA/GFDL, Princeton, USA, 1999.

Palmer, J. R. and Totterdell, I. J.: Production and export in a global ocean ecosystem model, Deep-Sea Res. Pt. I, 48, 1169–1198, doi:10.1016/S0967-0637(00)00080-7, 2001.

Parekh, P., Joos, F., and Müller, S.: A modeling assessment of the interplay between aeolian iron fluxes and iron-binding ligands in controlling carbon dioxide fluctuations during Antarctic warm events, Paleoceanography, 23, PA4202, doi:10.1029/2007PA001531, 2008.

Petoukhov, V., Mokhov, I. I., Eliseev, A. V., and Semenov, V. A.: The IAP RAS global climate model, Dialogue-MSU, Moscow, Russia, 1998.

Petoukhov, V., Ganopolski, A., Brovkin, V., Claussen, M., Eliseev, A., Kubatzki, C., and Rahmstorf, S.: CLIMBER-2: a climate system model of intermediate complexity, Part I: model description and performance for present climate, Clim. Dynam., 16, 1–17, doi:10.1007/PL00007919, 2000.

Petoukhov, V., Claussen, M., Berger, A., Crucifix, M., Eby, M., Eliseev, V., Fichefet, T., Ganopolski, A., Goosse, H., Kamenkovich, I., Mokhov, I. I., Montoya, M., Mysak, L. A., Sokolov, A., Stone, P., Wang, Z., and Weaver, A. J.: EMIC Intercomparison Project (EMIP-CO_2): comparative analysis of EMIC simulations of climate, and of equilibrium and transient responses to atmospheric CO_2 doubling, Clim. Dynam., 25, 363–385, doi:10.1007/s00382-005-0042-3, 2005.

Plattner, G.-K., Knutti, R., Joos, F., Stocker, T. F., von Bloh, W., Brovkin, V., Cameron, D., Driesschaert, E., Dutkiewicz, S., Eby, M., Edwards, N. R., Fichefet, T., Hargreaves, J. C., Jones, C. D., Loutre, M. F., Matthews, H. D., Mouchet, A., Müller, S. A., Nawrath, S., Price, A., Sokolov, A., Strassman, K. M., and Weaver, A. J.: Long-term climate commitments projected with climate-carbon cycle models, J. Climate, 21, 2721–2751, doi:10.1175/2007JCLI1905.1, 2008.

Pongratz, J., Reick, C., Raddatz, T., and Claussen, M.: A reconstruction of global agricultural areas and land cover for the last millennium, Global Biogeochem. Cy., 22, GB3018, doi:10.1029/2007GB003153, 2008.

Pope, V. D., Gallani, M. L., Rowntree, P. R., and Stratton, R. A.: The impact of new physical parameterizations in the Hadley Centre climate model: HadAM3, Clim. Dynam., 16, 123–146, doi:10.1007/s003820050009, 2000.

Rahmstorf, S., Crucifix, M., Ganopolski, A., Goosse, H., Kamenkovich, I., Knutti, R., Lohmann, G., Marsh, R., Mysak, L. A., Wang, Z., and Weaver, A. J.: Thermohaline circulation hysteresis: a model intercomparison, Geophys. Res. Lett., 32, L23605, doi:10.1029/2005GL023655, 2005.

Reader, M. C. and Boer, G. J.: The modification of greenhouse gas warming by the direct effect of sulphate aerosols, Clim. Dynam., 14, 593–607, doi:10.1007/s003820050243, 1998.

Ridgwell, A. and Hargreaves, J.C.: Regulation of atmospheric CO_2 by deep-sea sediments in an Earth system model, Global Biogeochem. Cy., 21, GB2008, doi:10.1029/2006GB002764, 2007.

Ridgwell, A., Hargreaves, J. C., Edwards, N. R., Annan, J. D., Lenton, T. M., Marsh, R., Yool, A., and Watson, A.: Marine geochemical data assimilation in an efficient Earth System Model of global biogeochemical cycling, Biogeosciences, 4, 87–104, doi:10.5194/bg-4-87-2007, 2007.

Ritz, S. P., Stocker, T. R., and Joos, F.: A coupled dynamical ocean-energy balance atmosphere model for paleoclimate studies, J. Climate, 24, 349–375, doi:10.1175/2010JCLI3351.1, 2011.

Sabine, C., Feely, R. A., Gruber, N., Key, R. M., Lee, K., Bullister, J. L., Wanninkhof, R., Wong, C. S., Wallace, D. W. R., Tilbrook, B., Millero, F. J., Peng, T.-H., Kozyr, A., Ono, T., and Rios, A. F.: The oceanic sink for anthropogenic CO_2, Science, 305, 367–371, doi:10.1126/science.1097403, 2004.

Schleussner, C. F. and Feulner, G.: A volcanically triggered regime shift in the subpolar North Atlantic ocean as a possible origin of the Little Ice Age, Clim. Past Discuss., 8, 6199–6219, doi:10.5194/cpd-8-6199-2012, 2012.

Schmidt, G. A., Jungclaus, J. H., Ammann, C. M., Bard, E., Braconnot, P., Crowley, T. J., Delaygue, G., Joos, F., Krivova, N. A., Muscheler, R., Otto-Bliesner, B. L., Pongratz, J., Shindell, D. T., Solanki, S. K., Steinhilber, F., and Vieira, L. E. A.: Climate forcing reconstructions for use in PMIP simulations of the Last Millennium (v1.1), Geosci. Model Dev., 5, 185–191, doi:10.5194/gmd-5-185-2012, 2012.

Schmittner, A., Oschlies, A., Matthews, H. D., and Galbraith, E. D.: Future changes in climate, ocean circulation, ecosystems and biogeochemical cycling simulated for a business-as-usual CO_2 emission scenario until year 4000 AD, Global Biogeochem. Cy., 22, 1013–1034, doi:10.1029/2007GB002953, 2008.

Schneider, D. P., Ammann, C. M., Otto-Bliesner, B. L., and Kaufman, D. S.: Climate response to large, high-latitude and low-latitude volcanic eruptions in the Community Climate System Model, J. Geophys. Res., 114, D15101, doi:10.1029/2008JD011222, 2009.

Servonnat, J., Yiou, P., Khodri, M., Swingedouw, D., and Denvil, S.: Influence of solar variability, CO_2 and orbital forcing between 1000 and 1850 AD in the IPSLCM4 model, Clim. Past, 6, 445–460, doi:10.5194/cp-6-445-2010, 2010.

Severijns, C. A. and Hazeleger, W.: The efficient global primitive equation climate model SPEEDO V2.0, Geosci. Model Dev., 3, 105–122, doi:10.5194/gmd-3-105-2010, 2010.

Shaffer, G. and Sarmiento, J. L.: Biogeochemical cycling in the global ocean: 1. A new, analytical model with continuous vertical resolution and high-latitude dynamics, J. Geophys. Res., 100, 2659–2672, 1995.

Shaffer, G., Malskær Olsen, S., and Pepke Pedersen, J. O.: Presentation, calibration and validation of the low-order, DCESS Earth System Model (Version 1), Geosci. Model Dev., 1, 17–51, doi:10.5194/gmd-1-17-2008, 2008.

Shindell, D. T., Schmidt, G. A., Miller, R., and Mann, M. E.: Volcanic and solar forcing of climate change during the pre-industrial era, J. Climate, 16, 4094–4107, 2003

Sitch, S., Smith, B., Prentice, I. C., Arneth, A., Bondeau, A., Cramer, W., Kaplan, J. O., Levis, S., Lucht, W., Sykes, M. T., Thonicke, K., and Venevsky, S.: Evaluation of ecosystem dynamics, plant geography and terrestrial carbon cycling in the LPJ dynamic global vegetation model, Global Change Biol., 9, 161–185, doi:10.1046/j.1365-2486.2003.00569.x, 2003.

Six, K. D. and Maier-Reimer, E.: Effects of plankton dynamics on seasonal carbon fluxes in an ocean general circulation model, Global Biogeochem. Cy., 10, 559–583, doi:10.1029/96GB02561, 1996.

Smith, R. S.: The FAMOUS climate model (versions XFXWB and XFHCC): description update to version XDBUA, Geosci. Model Dev., 5, 269–276, doi:10.5194/gmd-5-269-2012, 2012.

Smith, R. S., Gregory, J. M., and Osprey, A.: A description of the FAMOUS (version XDBUA) climate model and control run, Geosci. Model Dev., 1, 53–68, doi:10.5194/gmd-1-53-2008, 2008.

Sokolov, A. P. and Stone, P. H.: A flexible climate model for use in integrated assessments, Clim. Dynam., 14, 291–303, doi:10.1007/s003820050224, 1998.

Sokolov, A. P., Schlosser, C. A., Dutkiewicz, S., Paltsev, S., Kicklighter, D. W., Jacoby, H. D., Prinn, R. G., Forest, C. E., Reilly, J., Wang, C., Felzer, B., Sarofim, M. C., Scott, J., Stone, P. H., Melillo, J. M., and Cohen, J.: The MIT Integrated Global System Model (IGSM) Version 2: Model description and baseline evaluation, MIT JP Report 124, Cambridge, USA, 2005.

Sokolov, A. P., Kicklighter, D. W., Melillo, J. M., Felzer, B. S., Schlosser, C. A., and Cronin, T. W.: Consequences of considering carbon-nitrogen interactions on the feedbacks between climate and the terrestrial carbon cycle, J. Climate, 21, 3776–3796, doi:10.1175/2008JCLI2038.1, 2008.

Steinacher, M.: Modeling changes in the global carbon cycle – climate system, Ph.D. thesis, University of Bern, Bern, Switzerland, 2011.

Stocker, B. D., Strassmann, K., and Joos, F.: Sensitivity of Holocene atmospheric CO_2 and the modern carbon budget to early human land use: analyses with a process-based model, Biogeosciences, 8, 69–88, doi:10.5194/bg-8-69-2011, 2011.

Stouffer, R. J., Yin, J., Gregoryn, J. M., Dixon, K. W., Spelman, M. J., Hurlin, W., Weaver, A. J., Eby, M., Flato, G. M., Hasumi, H., Hu, A., Jungclaus, J. H., Kamenkovich, I. V., Levermann, A., Montoya, M., Murakami, S., Nawrath, S., Oka, A., Peltier, W. R., Robitaille, D. Y., Sokolov, A., Vettoretti, G., and Weber, S. L.: Investigating the causes of the response of the thermohaline circulation to past and future climate changes, J. Climate, 19, 1365–1387, doi:10.1175/JCLI3689.1, 2006.

Strassmann, K. M., Joos, F., and Fischer, G.: Simulating effects of land use changes on carbon fluxes: past contributions to atmospheric CO_2 increases and future commitments due to losses of terrestrial sink capacity, Tellus B, 60, 583–603, doi:10.1111/j.1600-0889.2008.00340.x, 2008.

Swingedouw, D., Terray, L., Cassou, C., Voldoire, A., Salas-Meìlia, D., and Servonnat, J.: Natural forcing of climate during the last millennium: fingerprint of solar variability, Clim. Dynam., 36, 1–16, 2010.

Tachiiri, K., Hargreaves, J. C., Annan, J. D., Oka, A., Abe-Ouchi, A., and Kawamiya, M.: Development of a system emulating the global carbon cycle in Earth system models, Geosci. Model Dev., 3, 365–376, doi:10.5194/gmd-3-365-2010, 2010.

Taylor, K. E., Stouffer, R. J., and Meehl, G. A.: An overview of CMIP5 and the experiment design, B. Am. Meteorol. Soc., 93, 485–498, doi:10.1175/BAMS-D-11-00094.1, 2012.

Tschumi, T., Joos, F., and Parekh, P.: How important are southern hemisphere wind changes for low glacial carbon dioxide? A model study, Paleoceanography, 23, PA4208, doi:10.1029/2008PA001592, 2008.

Tschumi, T., Joos, F., Gehlen, M., and Heinze, C.: Deep ocean ventilation, carbon isotopes, marine sedimentation and the deglacial CO_2 rise, Clim. Past, 7, 771–800, doi:10.5194/cp-7-771-2011, 2011.

Wang, Y.-M., Lean, J. L., and Sheeley Jr., N. R.: Modeling the Sun's magnetic field and irradiance since 1713, Astrophys. J., 625, 522–538, doi:10.1086/429689, 2005.

Wania, R., Ross, I., and Prentice, I. C.: Integrating peatlands and permafrost into a dynamic global vegetation model: 1. Evaluation and sensitivity of physical land surface processes, Global Biogeochem. Cy., 23, GB3014, doi:10.1029/2008GB003412, 2009a.

Wania, R., Ross, I., and Prentice, I. C.: Integrating peatlands and permafrost into a dynamic global vegetation model: 2. Evaluation and sensitivity of vegetation and carbon cycle processes, Global Biogeochem. Cy., 23, GB3015, doi:10.1029/2008GB003413, 2009b.

Weaver, A. J., Eby, M., Wiebe, E. C., Bitz, C. M., Duffy, P. B., Ewen, T. L., Fanning, A. F., Holland, M. M., MacFadyen, A., Saenko, O., Schmittner, A., Wang, H., and Yoshimori, M.: The UVic earth system climate model: Model description, climatology, and applications to past, present and future climates, Atmos.-Ocean, 39, 361–428, doi:10.1080/07055900.2001.9649686, 2001.

Weaver, A. J., Eby, M., Kienast, M., and Saenko, O. A.: Response of the Atlantic meridional overturning circulation to increasing atmospheric CO_2: Sensitivity to mean climate state, Geophys. Res. Lett., 34, L05708, doi:10.1029/2006GL028756, 2007.

Williamson, M. S., Lenton, T. M., Shepherd, J. G., and Edwards, N. R.: An efficient numerical terrestrial scheme (ENTS) for Earth system modeling, Ecol. Model., 198, 362–374, 2006.

Wright, D. G. and Stocker, T. F.: Sensitivities of a zonally averaged global ocean circulation model, J. Geophys. Res., 97, 12707–12730, doi:10.1029/92JC01168, 1992.

Zeng, N.: Glacial-interglacial atmospheric CO_2 change – the glacial burial hypothesis, Adv. Atmos. Sci., 20, 677–693, 2003.

Zeng, N., Neelin, J. D., and Chou, C: The first quasi-equilibrium tropical circulation model – implementation and simulation, J. Atmos. Sci., 57, 1767–1796, 2000.

Zeng, N., Qian, H., Munoz, E., and Iacono, R.: How strong is carbon cycle-climate feedback under global warming?, Geophys. Res. Lett., 31, L20203, doi:10.1029/2004GL020904, 2004.

Zeng, N., Mariotti, A., and Wetzel, P.: Terrestrial mechanisms of interannual CO_2 variability, Global Biogeochem. Cy., 19, GB1016, doi:10.1029/2004GB002273, 2005.

Zickfeld, K., Eby, M., Matthews, H. D., Schmittner, A., and Weaver, A. J.: Nonlinearity of carbon cycle feedbacks, J. Climate, 24, 4255–4275, 2011.

Zickfeld, K., Eby, M., Weaver, A. J., Crespin, E., Fichefet, T., Goosse, H., Philippon-Berthier, G., Edwards, N. R., Holden, P. B., Eliseev, A. V., Mokhov, I. I., Feulner, G., Kienert, H., Perrette, M., Schneider von Deimling, T., Forest, C. E., Joos, F., Spahni, R., Steinacher, M., Kawamiya, M., Tachiiri, K., Kicklighter, D., Monier, E., Schlosser, A., Sokolov, A. P., Matsumoto, K., Tokos, K., Olsen, S. M., Pedersen, J. O. P., Shaffer, G., Ridgwell, A., Zeng, N., and Zhao, F.: Long-term climate change commitment and reversibility, J. Climate, in press, 2013.